https://doi.org/10.5194/egusphere-2025-53
Preprint. Discussion started: 24 January 2025

Statistical analysis of ocean currents in the Eastern Mediterranean

Yosef Ashkenazy[1], Hezi Gildor[2], and Aviv Solodoch[2]

[1]Department of Environmental Physics, BIDR, Ben-Gurion University of the Negev, Midreshet Ben-Gurion, Israel
[2]The Institute of Earth Sciences, The Hebrew University of Jerusalem, Israel

Correspondence: Yosef Ashkenazy (ashkena@bgu.ac.il)

Abstract. We examined the probability density function (pdf) of current speeds in the Eastern Mediterranean Sea, near the central coast of Israel. The currents cover depths from the surface to over 1.3 km and span a period from November 2016 to March 2024. We estimated the parameters of three typical distributions that are usually used to model the pdfs of currents and wind speed; the Weibull, the General Extreme Value, and the Generalized Gamma. We find that the three-parameter Generalized Gamma distribution best describes the pdfs of the observed current speed series. Still, the studied current speed time series may not be long enough to assess the exact values of the underlying pdf, as some years exhibit stronger currents that affect the distribution. The time series of the difference between consecutive current speeds exhibit less long-term variability; we studied their statistics and found that the stretched exponential pdf describes better (than the normal distribution) their statistics. Comparison of the measured current speed pdfs to current speed pdfs of a high-resolution (1 km) regional circulation model (ROMS) and Copernicus Mediterranean reanalysis daily mean currents (~ 4.6 km resolution) indicates discrepancies from the data. Our results may help to improve statistical models for ocean currents and the estimation of extreme current events.

1 Introduction

The circulation of the ocean is a vital player in the climate system. It helps to regulate the climate system and is linked to far-reaching teleconnections. Ocean circulation played a significant role in past climate events and is expected to continue to do so in the changing climate of the future. The ocean's circulation and dynamics are driven by various sources, including surface winds, tides, and pressure gradients, which are also influenced by local temperature and salinity.

Various classical theories explain the characteristics and existence of ocean currents. These include the Ekman layer theory (Ekman, 1905) that describes the impact of winds on surface currents, the theories for Western boundary currents (Stommel, 1948; Munk, 1950), and the Stommel-Aron theory (Stommel and Arons, 1960) that explains the abyssal ocean circulation. However, since winds and currents are stochastic in nature (e.g., Seguro and Lambert, 2000; Chu, 2008a), they require statistical analysis and formulation. Indeed, many studies have performed statistical analyses of ocean currents and proposed statistical models to explain their observed statistical properties.

Being a main forcing of ocean currents and easier to observe, numerous studies have focused on investigating the statistical distribution of winds (e.g., Seguro and Lambert, 2000; Monahan, 2006a, b; Campisi-Pinto et al., 2020; Justus et al., 1978; Takle and Brown, 1978; Bowden et al., 1983; Conradsen et al., 1984; Troen and Petersen, 1989; Lun and Lam, 2000; Ulgen

https://doi.org/10.5194/egusphere-2025-53
Preprint. Discussion started: 24 January 2025

and Hepbasli, 2002; Monahan, 2006a, b; Carta et al., 2009; Kiss and Jánosi, 2008; Kelly et al., 2014; Drobinski et al., 2015), while less attention has been given to the statistical properties and distribution of ocean currents (Chu, 2008a, b; Ashkenazy and Gildor, 2011; Ashkenazy et al., 2016; Campisi-Pinto et al., 2020). Most of these studies concluded that the winds and currents follow the Weibull distribution (Justus et al., 1978; Takle and Brown, 1978; Bowden et al., 1983; Conradsen et al., 1984; Troen and Petersen, 1989; Lun and Lam, 2000; Seguro and Lambert, 2000; Ulgen and Hepbasli, 2002; Chu, 2008b; Manwell et al., 2010; Kelly et al., 2014). Yet, other studies used other distributions to model wind and current speed data (Tuller and Brett, 1984; Bauer, 1996; Carta and Ramirez, 2007; Morrissey and Greene, 2012; Bel and Ashkenazy, 2013; Campisi-Pinto et al., 2020).

Previous studies investigated the probability distribution of surface geostrophic current speed based on satellite altimetry data and found that these are Weibull distributed where different parts of the world ocean are characterized by different values of the shape and scale parameters (Smith and Gille, 1998; Chu, 2008b, 2009). Chu (2008a) analyzed the speed of the upper levels of the tropical Pacific Ocean and found that it follows the Weibull distribution within the top 50 meters. However, the distribution was found to be different at deeper levels. The same study also discovered that the parameters of the Weibull distribution change during El Nino and La Nina events. The statistics of the global ocean surface currents that were estimated based on altimetry data were analyzed using surrogate data tests; it was found that the generalized gamma (GG) distribution (a generalization of the Weibull distribution) better fits the probability distribution of the data (Campisi-Pinto et al., 2020).

In addition to the analysis of current speeds, previous studies have also examined the statistics of velocity components of surface currents (rather than current speed) based on altimetry data. It has been found that the distribution of the velocity components differs depending on the size of the ocean area being examined (Smith and Gille, 1998; Gille and Smith, 2000). When focusing on small ocean areas, the distribution appears to follow a Gaussian distribution, whereas considering the mean currents over extensive ocean areas, the probability appears to be an exponential distribution.

Coastal Ocean Dynamics Application Radar (CODAR) systems can estimate surface currents with high accuracy in both time (30 min-1 hour) and space (ranging from hundreds of meters to several kilometers). Laws et al. (2010) presented the probability distribution of these current velocities, but did not discuss the theoretical distribution that corresponds to these currents. CODAR-based surface current speeds at the Gulf of Eilat/Aqaba were estimated to follow the Weibull distribution (Ashkenazy and Gildor, 2011). This study introduced an Ekman layer model forced by local winds and additional stochastic geostrophic currents to reproduce the observed surface current pdf. It was also found that the spatial variability of the shape parameter of the Weibull distribution is larger in the Gulf of Eilat in comparison to the Nan-Wan Bay in Taiwan (Ashkenazy et al., 2016). Kabir et al. (2015) used the HYbrid Coordinate Ocean Model (HYCOM) and high-frequency radar data to study the statistics of the Gulf Stream current and concluded that the Weibull distribution underlies the current speed distribution.

The statistics of sub-surface and deep ocean currents received lesser attention than the surface currents. This is mainly due to the lack of long, continuous, measured ocean currents. Paquette (1972) analyzed a series of relatively short-time current data from various depths and locations and found that the logarithm of the current speed is approximately normally distributed. Chu (2008a) studied the current speed distribution of the tropical Pacific and found that the currents in the upper 50 m follow the Weibull distribution, unlike the deeper currents of 100 m to 200 m. Another study (Bracco et al., 2000a) used barotropic

https://doi.org/10.5194/egusphere-2025-53
Preprint. Discussion started: 24 January 2025

ocean turbulence numerical simulations to investigate the velocity distribution inside and outside coherent structures. These authors also used observations (Bracco et al., 2000b) and numerical simulations (Bracco et al., 2003) of the North Atlantic to study the probability distribution of the Lagrangian current and found that the velocity components do not follow the Gaussian distribution but the exponential distribution; this finding may have implications on the parameterization of particle dispersion.

The present study aims to investigate the statistical characteristics of the current speed time series and to deduce the pdf associated with these time series. Our analysis is based on data collected over 7 years of current meters deployment in a mooring site (named "DeepLev") in the Levantine basin of the East Mediterranean Sea), at the foot of the continental slope offshore of Israel (Katz et al., 2020); see Fig. 1. We find that among the Weibull distribution, the General Extreme Value (GEV) distribution, and the Generalized Gamma (GG) distribution, the latter is the best for modeling the statistics of the current speeds. We also analyzed the statistics of current speed increments and found that the stretched exponential distribution better fits the data than the normal distribution. Analysis of the currents of high-resolution oceanic general circulation (OGCM) simulations of the Mediterranean Sea (Solodoch et al., 2023) and Copernicus oceanic reanalysis (Escudier et al., 2020) indicate differences from the data.

Below we first describe the data and methods used in this study (Sec. 2). We then present the results (Sec. 3) and provide a summary and conclusions (Sec. 4).

2 Data and methods

2.1 Studied area and Data

The circulation of the Mediterranean Sea has been studied extensively in the past decades (e.g., Malanotte-Rizzoli et al., 2014, and references therein). The Mediterranean Sea is connected to the global ocean (Atlantic Ocean) through the Straits of Gibraltar where relatively cold and fresh flow to the Mediterranean Sea at the surface layer. This water becomes warmer, saltier, and heavier while flowing along the southern coast of the Mediterranean Sea to the Levantine basin and the eastern part of the Mediterranean Sea; the Levantine surface water is warmer by 3-4°C (Shaltout and Omstedt, 2014) and saltier by ∼16 ppt (Ferguson et al., 2008) than the water entering the Gibraltar Straits. Then the water completes the circulation back to the Gibraltar Straits through intermediate water levels along the northern parts of the Mediterranean Sea and exits back to the Atlantic Ocean through the lower parts of the Gibraltar Straits (Bergamasco and Malanotte-Rizzoli, 2010; Tanhua et al., 2013; Malanotte-Rizzoli et al., 2014). The deep water formation in the Mediterranean Sea exhibited drastic and rapid changes (the Eastern Mediterranean transient) (Roether et al., 1996) and was studied using observation and models (e.g., Ashkenazy et al., 2012; Malanotte-Rizzoli et al., 2014; Amitai et al., 2017, 2019; Mavropoulou et al., 2022; Parras-Berrocal et al., 2022, 2023; Pinardi et al., 2023).

A deep-water mooring, the DeepLev, was recently installed in the Levantine Basin of the Eastern Mediterranean (Katz et al., 2020). The mooring location is about 50 km offshore of Haifa (Israel), at a depth of 1.5 km; its coordinates are 33.0618°N, 34.4888°E. The DeepLev mooring was used to gather data about the water's physical, chemical, and biological properties at

https://doi.org/10.5194/egusphere-2025-53
Preprint. Discussion started: 24 January 2025

different depths, as well as sediment transport. These measurements were taken from November 2016 onward. In this study, we focus on the current measurements of the DeepLev.

DeepLev data was used to study several aspects of ocean dynamics in the Eastern Mediterranean Sea. Katz et al. (2020) described the data collected at the DeepLev mooring and also estimated the sedimentation flux at this region. This study concluded that continental sediment can reach distances larger than 100 km offshore. Another study (Feliks et al., 2022) analyzed the DeepLev current velocity and found upper ocean oscillations that are much stronger and much slower than the tidal oscillations. DeepLev current and pressure data was also used to study tidal variability in this region (Mantel et al., 2024). It was found that the semi-diurnal and diurnal tides vary seasonally. An additional study (Haim et al., 2023) used the DeepLev mooring station to measure surface wave patterns and dynamics. A recent modeling study of the Eastern Mediterranean Sea compared velocity spectra from DeepLev to the model's simulations (Solodoch et al., 2023).

We consider the DeepLev current velocity measured by Acoustic Doppler Current Profilers (ADCPs) which were mounted at depths of 30 m, 100 m, and 400 m. From these ADCPs, we analyzed the current velocities of depths 10, 45, 80, 160, and 430 m. In addition, we used a single-point current measurement at a depth of 1300 m. For more details on the instruments, see Table 1 of Katz et al. (2020). The selected depths roughly represent the different parts of the water column: the mixed layer, the thermocline, and the deep ocean. The data we analyzed covers the time period from Nov. 14 2016 to March 5, 2024. Data were collected through nine consecutive deployments. In two deployments the 10 m instrument failed, and in one deployment, the instrument intended for 1300 m depth was placed at a depth of 800 m and thus is ignored here. These gaps and the gaps between the different deployments were ignored in the statistical analysis. The different instruments were recorded using different sampling rates during the different deployments, and we resampled them to the longest sampling time of two hours.

In addition to the analysis of the measured data, we also analyzed the currents of a state-of-the-art oceanic general circulation model (Solodoch et al., 2023). These authors used the Coastal and Regional Ocean Community (CROCO) model (Debreu et al., 2012) that is based on the Regional Oceanic Modeling System (ROMS) (Shchepetkin and McWilliams, 2005). The model was forced by realistic atmospheric fields and reanalysis currents (Escudier et al., 2020) that were used to simulate the time period between 2017 and 2019 using 3 km lateral resolution, the time period between Feb. 2017 to Dec. 2018 using 1 km resolution, and the winter and summer of 2018 using 300 m resolution. For a comparison of DeepLev velocity spectra with the model, see Solodoch et al. (2023). Below, we focus on the 1 km model simulation as this simulation has both fine resolution and long simulation time; unfortunately, the CROCO simulations are highly time-consuming such that we were unable to simulate the entire time of the DeepLev measured data. The temporal resolution of the 1 km resolution data is 2 h, the same as the resampling rate of the data.

The simulation described in the previous paragraph does not span the temporal extent of the measured DeepLev data. We thus also analyzed the Copernicus Marine Environment Monitoring Service (CMEMS) reanalysis (Escudier et al., 2020). We consider the same time period as the data (Nov. 14 2016 to March 5, 2024); the Copernicus currents are daily average, and we thus used the daily mean current speed of the data to compare the two.

https://doi.org/10.5194/egusphere-2025-53
Preprint. Discussion started: 24 January 2025

2.2 Methods

In this study, we examine three pdfs, the Weibull, the General Extreme Value (GEV), and Generalized Gamma (GG) distributions, as possible statistical distributions of current speeds.

The Weibull distribution is a two-parameter pdf defined as:

$$f(x>0) = \frac{k}{\lambda}\left(\frac{x}{\lambda}\right)^{k-1} e^{-(x/\lambda)^k}, \tag{1}$$

where λ is the scale parameter (here has units of speed) and k is the (dimensionless) shape parameter. $k = 1$ reduces the Weibull distribution to the exponential distribution while $k = 2$ reduces the Weibull distribution to the Rayleigh distribution.

The GEV distribution is a three-parameter pdf defined as:

$$f(x) = \frac{1}{\sigma} t(x)^{k+1} e^{-t(x)}, \tag{2}$$

where

$$t(x) = \begin{cases} \left(1 + k\left(\frac{x-\mu}{\sigma}\right)\right)^{-1/k}, & \text{if } k \neq 0 \\ e^{-(x-\mu)/\sigma}, & \text{if } k = 0, \end{cases} \tag{3}$$

and μ is the location parameter, σ is the scale parameter, and k is the shape parameter; in this study, the units of μ and σ are units of speed while k is dimensionless. The GEV distribution is the general pdf in extreme value theory and may be reduced to the Fréchet, Weibull, and Gumbel pdfs under appropriate assumptions.

The GG distribution is a three-parameter pdf defined as:

$$f(x>0) = \frac{1}{\Gamma(\varepsilon)} \frac{k}{\lambda}\left(\frac{x}{\lambda}\right)^{\varepsilon k - 1} e^{-(x/\lambda)^k}, \tag{4}$$

where Γ is the gamma function, λ is the scale parameter (here with speed units), and k, ε are the dimensionless shape parameters. The GG pdf reduces to the Weibull pdf when $\varepsilon = 1$. We use the maximum likelihood method to fit the theoretical pdf (model) to the data.

In addition to the above three pdfs, we used the normal and stretched exponential (or the generalized normal distribution) pdfs to model the current speed increment time series. The normal distribution is defined as

$$f(x) = \frac{1}{\sqrt{2\pi}\sigma} e^{-\frac{x^2}{2\sigma^2}}, \tag{5}$$

where σ^2 is the variance of the distribution. The location parameter of the normal distribution (the mean) μ is not included here as the current speed increment time series are stationary and the mean of the distribution is very close to zero. The stretched exponential (generalized normal distribution) pdf is defined as

$$\frac{1}{2\sigma\Gamma\left(1+\frac{1}{\beta}\right)} e^{-|\frac{x}{\sigma}|^\beta} \tag{6}$$

https://doi.org/10.5194/egusphere-2025-53
Preprint. Discussion started: 24 January 2025

where σ is scale parameter and β is the shape parameter. The stretched exponential pdf takes the form of exponential pdf when $\beta = 1$ and the form of normal pdf when $\beta = 2$.

We examine here two and three-parameter pdfs and it is necessary to determine, for example, whether the two-parameter Weibull pdf exhibits similar performance as the three-parameter pdf or not. Naturally, one expects the three-parameter pdf to yield a better fit to the observed distribution simply since it has one additional parameter. The likelihood ratio test (Davidson et al., 2004) aims to determine whether the more complex pdf, which has more parameters, significantly outperforms the fit to the histogram of the data when using the simpler pdf with fewer parameters. In other words, the likelihood ratio test determines whether the data significantly favor the pdf with the more parameters in comparison to the fewer parameter pdf. The likelihood ratio test may be applied when the pdf with the fewer parameters is a subset of the pdf that has more parameters. We use this test to verify whether the GG pdf exhibits a significantly better fit than the Weibull pdf.

In addition to the likelihood ratio test, we quantify the difference Δ between the distribution of the data and the pdf of the theoretical pdfs by calculating the square root of the mean of the square of the difference between the distribution of the data and the fitted pdf. To examine more precisely the tail of the distribution, we repeated the analysis after taking the log of the pdf. Smaller Δ values indicate a better fit of the theoretical pdf to the observed one.

3 Results

3.1 Measured currents

The current speed time series analyzed here are presented in Fig. 2. We first note that there are gaps in the data; these gaps are due to the lapse between the different deployments and due to errors or instrument failures in some deployments (in two deployments for the 10 m depth instrument and in one deployment for the 1300 m depth instrument). The current time series of the upper four depths exhibit similar behavior with a “noisy” pattern superimposed on slow modulations. The slow modulations seem to be associated with winter storms which extend well below the mixed layer (see Fig. 7c of Solodoch et al., 2023, for the depth of the mixed layer). The slow modulations are less evident in the deeper stations of depths 430 m and 1300 m. As expected, the mean and the standard deviation of the current series decrease with depth. We present the correlation between the time series of the different depths in Fig. 3. This figure shows that the correlation between the time series of the different depths is significant (Fig. 3b). As expected, the correlation decreases when the depth distance becomes larger (Fig. 3c,d). Moreover, the correlation decreases with time lag slowly (tens of days Fig. 3b), indicating that the current speed time series exhibits slow modulations, possibly due to seasonal effects or mesoscale eddies. The correlation between the surface current and the deep ocean suggest energy injection from the surface.

Next, we construct the pdf of the current speed time series of the different depths. These are plotted in Fig. 4, both in regular (left panels) and semi-log (right panels) plots. The latter aims to emphasize the tail of the distribution, which presents information regarding extreme current speed events. We fitted the Weibull, GEV, and GG pdfs to the observed distributions. The three parameters GEV and GG pdfs seem to exhibit a better fit than the two-parameter Weibull pdf; both for the central part of the distribution and the tails, the Weibull pdf falls below the observed distribution as well as below the pdfs of the two

https://doi.org/10.5194/egusphere-2025-53
Preprint. Discussion started: 24 January 2025

other three parameter pdfs. We will quantify the performance of the different pdfs below. When focusing on the right tail of the distribution, it is apparent that the GG distribution exhibits the best fit to the data and it is situated between the lower estimate of the Weibull distribution and the upper estimate of the GEV distribution.

We summarize the parameters of the three fitted pdfs in Fig. 5; the fitted parameters of the data are represented by the blue circles. The λ parameter of the Weibull distribution is the scale parameter and, as expected, decreases with depth, similar to the mean current speed. The k shape parameter of the Weibull distribution is less than 1.8 and larger than 1.3, indicating that the tail of the distribution decays faster than exponential decay.

The second row of Fig. 5 displays the GEV distribution parameters; the parameters of the data are indicated by the blue circles. μ and σ are the location and scale parameters and decrease with depth, similar to the mean and std of the data (included at the top-left corner of the panels of Fig. 2). The k parameter is positive and smaller than 0.4. Larger k values indicate slower decay of the tail of the distribution.

The fitted parameters of the GG distribution are summarized in the third row of Fig. 5 (blue circles); see also the titles of the right column panels of Fig. 4. Here, the scale parameter λ does not always reflect the decrease of the mean current speed with depth. The k shape parameter exhibits much smaller variability ($0.5 \lesssim k \lesssim 1.8$) in comparison to ε ($0 < \varepsilon < 8$). Such a larger range of ε indicates that the observed pdf exhibits considerable irregularities. This is also expressed in the interannual variability of the estimated GG parameter; see Fig. A13. Interestingly, the shape parameters of all the distributions (k and ε) change monotonically from the surface to depth 160 m but their trend is reversed between the depths of 430 m and 1300 m.

We next examine whether the three-parameter GG pdf better models the current speed data in comparison to the two-parameter Weibull pdf; these two pdfs are nested, i.e., the GG pdf reduces to the Weibull pdf when $\varepsilon = 1$. For this purpose, we use the likelihood ratio test. We find, for all depths except the deepest location, that the null hypothesis is rejected such that the GG pdf provides a better description of the data; for the deepest location, the Weibull and GG pdfs exhibit a similar fit (see Fig. 4) and the null hypothesis that the pdfs are similar is not rejected. We thus conclude that GG pdf more correctly models the current speed statistics.

We next present the results of another test that quantifies the performance of the fitted pdfs. As described in Sec. 2, we calculate the Δ measure (i.e., the square root of the sum of the square difference), based on the observed and the fitted pdfs, both on regular and semi-log plots. The results are depicted in the top panels of Fig. 6, where the left panel plots the Δ values that are based on a regular plot, and the right panel shows the Δ values that are calculated based on a semi-log plot. Smaller Δ indicates a better fit of the proposed pdfs. We obtain the smallest Δ for the GG pdf (yellow circles), almost for all depths when calculated using a regular plot. On semi-log scales, however, the results are more complex where both the GG and GEV pdfs seem to be acceptable models for the tail of the distributions. Overall, our results suggest that GG pdf is the best pdf (among the three studied here) to model the current speed pdfs at all depths.

3.2 1 km resolution model

As mentioned in Sec. 2, Solodoch et al. (2023) performed state-of-the-art simulations of the Eastern Mediterranean Sea, spanning the initial part of the DeepLev measurements. The simulated current time series are plotted in Fig. A1 and exhibit a

https://doi.org/10.5194/egusphere-2025-53
Preprint. Discussion started: 24 January 2025

smoother pattern than the measured currents shown in Fig. 2. These different patterns result in current distributions (Fig. A2) that are different than the observations (Fig. 4). This difference is expressed by the different values of the fitted parameters that are based on the model (red circles in Fig. 5) in comparison to those of the observations (blue circles in Fig. 5); note that the difference is substantial as indicated by the non-overlapping error bars that represent the 5-95% confidence interval. However, the Δ measure plotted in the second row of Fig. 6 indicates that the GG pdf is the best to fit the model's currents when calculating the Δ on a regular plot, similar to the data (top left panel of Fig. 6). When focusing on the tails of the distributions (right panel on the second row of Fig. 6), the GEV shows the lowest Δ, suggesting it best describes the model's current speed extreme events. We obtained different results for the measured currents (top right panel of Fig. 6). Following the above, it is apparent that the numerical simulation of Solodoch et al. (2023) does not reproduce all the statistical characteristics of the measured current speed time series.

Since the time series of the 1-km resolution model is much shorter than measured data we also analyzed the data and model time series that share the common times of both; i.e., the intersection of the time series presented in Figs. 2 and A1. The pdfs of these time series are presented in Fig. A3, both using regular and semi-log plots. This figure indicates that: (a) The distributions of the data are concentrated to the left in comparison to the model's distributions, almost for all depths (left column of Fig. A3). This shift becomes smaller with depth and even reversed for the deepest time series. The above is consistent with the mean currents that are larger for the model in comparison to the data. (b) As a consequence of the above, the model exhibits larger and more frequent extreme current events (right column of Fig. A3).

We also computed the optimal parameters of the three pdfs studied here (Weibull, GEV, and GG) of the data and 1-km model common time current time series. The results are presented in Fig. A4 and also here, similar to Fig. 5, the fitted parameters of the data are different than those of the model. We also perform the Δ analysis of Fig. 6 for these time series. The results are presented in Fig. A5 and lead to the same conclusion we reached based on the original analysis shown in Fig. 6, that the GG pdf better describes the central part of the distribution of both the data and model and that the tail of the data distribution is better fitted by the GG pdf for some depths and by the GEV for other depths where for the 1-km resolution model the better pdf is GEV. We thus conclude that the shorter length of the model time series does not underlie the differences between the data and the model.

To pinpoint the source for the difference between the statistics of the measured currents and the statistics of the model's currents we added noise (with amplitude of 3 cm/s, $\sim$10%) to the model's current components, to mimic possible instrumental noise and subgrid turbulence. This did not result in a better correspondence between the data and the model. We next replaced parts of the Fourier transform of the model with that of the data, to find which part of the spectrum underlies the difference between the measured data statistics and the model's statistics. We find that when replacing the low frequencies (i.e., frequencies that are less than 10% of the inertial frequency) of the model with the low frequencies of the data, the statistical properties of these current speed time series become similar to that of the data. This indicates that the difference between the statistical properties of the data and the model lies in the low-frequency dynamics of the model, possibly suggesting that the slow eddy dynamics of the model are somehow different than that of the data.

https://doi.org/10.5194/egusphere-2025-53
Preprint. Discussion started: 24 January 2025

3.3 Daily mean measured current and Copernicus reanalysis

The 1 km resolution model (Solodoch et al., 2023) is forced by the Copernicus reanalysis (Escudier et al., 2020) whose spatial resolution is much coarser (4.6 km). Yet, unlike the 1 km resolution model, the Copernicus reanalysis spans the entire period of the data. The available Copernicus files are daily mean data (Fig. A7) and we compare it to the daily mean data (Fig. A6). Visually, these two sets of daily mean currents are similar; a noticeable exception is the current speeds of 2022 for which the observed currents are stronger than the reanalysis Copernicus currents. The similarity between the two datasets is expressed in the similarity in their pdfs (Fig. A8). Still, the distributions of the deepest location of 1300 m are less similar. Moreover, for almost all depths (except the depth of 430 m), extreme events are more probable for the data, as expressed by the higher blue (data) bars at the tails of the distributions. For the 1 km resolution model pdfs (Fig. A3), we observed the opposite, i.e., the model exhibited a higher probability of extreme events than the data.

We also estimated the parameters of the Weibull, GEV, and GG pdfs for the daily mean current and Copernicus reanalysis daily mean current (Fig. 7) and find that the data parameters are sometimes similar to the Copernicus parameters (mainly for the scale parameter, λ of the Weibull pdf, σ and μ of the GEV pdf, and to some extent λ of the GG pdf) and sometimes different (for the shape parameter k and partially for ε). The similarity in the scale parameters is consistent with the similar averages of the current means (included in the top right corner in Figs. A6 and A7).

We repeated the calculation of the Δ measure on the daily mean currents discussed above. The results are presented in the top four bottom panels of Fig. 6. The conclusion with regards to the best pdf to model the current speed time series remains unchanged, although the actual Δ values are not the same. I.e., also here, as for the conclusion based on the original data and 1 km resolution model, the central part of the distribution is best modeled by the GG pdf (both for the data and model) while for the tail of the distribution, for the measured currents sometimes the GEV pdf is best to fit the data, where in other times the GG pdf is the best to fit the data while for the model the GEV pdf is the best model.

Based on the above, the Copernicus 4.6 km resolution reanalysis better represents the statistical properties of the observed data, in comparison to the 1 km resolution forward model of Solodoch et al. (2023). On the one hand, this is expected as the fundamental difference between these model types is that the reanalysis state is continuously "nudged" during its evolution to better agree with observational data. On the other hand, ideally, the higher resolution model should provide a more accurate representation of the observations. However, the relevant bias of the 1 km model was in frequencies shorter than 10 inertial days, i.e., likely large-scale (mesoscale or basin-scale) currents, and their source may not necessarily be related to the fine resolution.

3.4 Current speed increment time series

Strong unusual currents like those of 2022 (Fig. 2) can affect the estimation of the fitted parameters. This is expressed by the different fitted parameters of the shorter observed current series presented in Fig. A4 (blue circles) in comparison to the entire series presented in Fig. 5. This suggests that longer current time series are needed for a more reliable estimation of the pdf parameters. Still, the temporal variations of the current speed are more stationary and the study of their statistical properties

https://doi.org/10.5194/egusphere-2025-53
Preprint. Discussion started: 24 January 2025

may help to model ocean dynamics when including stochastic components. In other words, the equations of motion describe Newton's laws in terms of acceleration (the time derivative or the increments of the velocity). We thus study below the statistical properties of the current speed increment time series.

We first present the distribution of the current speed increments time series in Fig. 8, both in regular and semi-log plots. We used the normal [Eq. (5)] and stretched exponential [Eq. (6)] pdfs to fit the distribution of the data and found that the stretched exponential pdf better fit the data, both for the central part of the distribution (left column of Fig. 8) and the tail of the distribution (right column of Fig. 8). It is evident that the tail of the distribution decays slower than the tail of the normal pdf ($\beta = 2$) but faster than the exponential pdf ($\beta = 1$). The exponent is between $1.1 \leq \beta \leq 1.4$ except for the deepest time series for which the exponent is $\beta = 1.8$. We observed similar behavior for the 1 km resolution current speed increment time series (Fig. A9). Yet, it is clear the speed increments in the model are smaller than those of the data, especially for the deeper locations (Fig. A10).

We summarize the estimated parameters of the stretched exponential and normal pdfs in Figs A11 and A12 respectively. As expected, the scale parameter σ of the stretched exponential pdf decreases with depth (upper left panel of Fig. A11) both for the data (blue) and model (red), although the model values are significantly lower than those of the data. This indicates that the model's variations are significantly smaller than those of the data; see also Fig. A10. The difference between the data and the model becomes smaller, yet significant when considering the time series that share the common times (lower left panel of Fig. A11). The exponent β is larger for the data, indicating that the tail of the distribution decays faster for the measured data than the current speed increment time series of the model (right panels of Fig. A11).

For $\beta = 2$, the stretched exponential pdf takes the form of normal distribution–we present the estimated σ parameter (standard deviation) of the normal distribution in Fig. A12. We find that σ decreases with depth, as expected and similar to the σ parameter of the stretched exponential pdf (Fig. A11). Also here, similar to the stretched exponential pdf, the values of the data are larger than those of the 1 km resolution model parameter (right panel of Fig. A12). When considering the time series of the common times and the data and model, the parameter values of the data and the model are very similar.

Here we considered two pdfs to fit the current speed increment time series and found that the stretched exponential pdf better fits the histograms than the normal pdf, both the data and model. Yet, even the stretched exponential pdf seems to underestimate the tail of the observed histograms (see the right column panels of Figs. 8,A9) such that other pdfs may better fit the current speed increment time series.

4 Summary and discussions

We analyzed the probability distribution of the current speed time series of the DeepLev station which is located in the Levantine basin of the Mediterranean Sea, close to the coast of Israel. The current speed time series span the depth of the water column, from the surface to a depth of 1.3 km. We consider three pdfs that were previously used to model current and wind speed time series: the two-parameter Weibull pdf, and the three-parameter GEV and GG pdfs. We find that the GG pdf best represents the current speed time series, across both the pdf central part and the tail.

https://doi.org/10.5194/egusphere-2025-53
Preprint. Discussion started: 24 January 2025

We also analyzed a high-resolution regional model (Solodoch et al., 2023) and found that the GG pdf best fits the central part of the distribution of the simulated currents, while the tail of the distribution better fitted by the GEV pdf. Additionally, the model's pdf are shifted to the right in comparison to the data's pdfs, indicating that the model exhibits stronger currents than the data (Fig. A3). Replacing the low-frequency amplitudes of the model's current time series with those of the data resulted in better correspondence to the observed current speed distribution. Additionally, we examined the daily mean currents of the Copernicus reanalysis (Escudier et al., 2020) and found the statistics of these to be closer to the data than the 1 km resolution model. Still, as with the 1 km resolution model, the central part of the distribution for the Copernicus reanalysis is also best fitted by the GG pdf, while the GEV pdf better fits the tail.

The interannual variations of the current speed are relatively large such that a long time series is needed to more accurately estimate the parameters of the fitted pdf. In other words, the interannual variability of the fitted parameters may also be relatively large. Still, the variability of the current speed time series is more stationary (not shown); we find that the distribution of the current speed increment time series follows the stretched exponential pdf, with tails decaying faster than exponential but slower than Gaussian. The current speed increments of the data are larger than those of the model, especially in the deep ocean. A stretched exponential stochastic process together with temporal correlations of the current speed time series may be used as a stochastic forcing in the equations of motion describing the internal dynamics of the ocean.

The climate in the Eastern Mediterranean exhibits seasonal variability, with cold, rainy, and stormy winters and hot, dry, and relatively calm summers. Ocean currents also vary seasonally with relatively stronger currents during the winter. Thus, one would expect that the statistical properties will be different during the winter and summer. Yet, since this seasonality is not strong and since there are gaps in the data (Fig. 2) we did not perform a separate seasonal analysis and considered the entire time series as one process.

Finding the theoretical pdf that best models the current speed data is important, e.g., for the estimation of the kinetic energy along the water column and for the estimation of power production. In addition, it may provide some knowledge regarding extreme current events. Yet, since the tail of the distribution is based on a few percent of the measurements, prediction of extreme events should be taken with caution, and, if possible, to estimate the uncertainty at the tails of the distribution.

The conclusion that the GG pdf is the best to fit the current speed time series of the DeepLev station is based on the analysis of three pdfs: Weibull, GEV, and GG. It is possible that other pdfs may better fit the current speed data. Yet, a better fit of four-parameter pdfs should be tested using the likelihood ratio test if possible, to ensure that the better fit is not only due to the increased numbers of parameters. The same holds for the current speed increment time series for which we find the two-parameter stretched exponential pdf to be the best fit. Although the analysis and conclusions of this study are based on the specific location, the DeepLev mooring, we speculate that some of our conclusions (e.g., that the GG pdf is a good fit for the current speed time series and that the current speed increments time series follows the stretched exponential pdf) are valid for other locations around the world ocean (see, e.g, Campisi-Pinto et al., 2020) and especially for the Eastern Mediterranean.

https://doi.org/10.5194/egusphere-2025-53
Preprint. Discussion started: 24 January 2025

Author contributions. YA conceptualized the research and the methodology, performed the analysis, prepared the figures, and wrote the manuscript. HG dealt with the data acquisition and AS provided the ROMS high-resolution simulation. All authors contributed to the methodology and the preparation of the final published paper.

Competing interests. The contact author has declared that none of the authors has any competing interests.

Acknowledgements. The operation of the DeepLev station was partially supported by the North American Friends of IOLR, the Mediterranean Sea Research Center of Israel (MERCI), and an ISF grant (No. 25/14) awarded to Yishai Weinstein and Ilana Berman-Frank. We express our gratitude to Yishai Weinstein, Ronen Alkalay, Timor Katz, Barak Herut, and Ilana Berman-Frank for their leadership in the DeepLev project. Special thanks go to the dedicated staff of IOLR, particularly Eli Biton and Tal Ozer, for their invaluable contributions to marine and technical operations. We also thank Yaron Toledo for providing some of the datasets used in this study, and Roy Barkan and Nadav Mantel for their insightful discussions.

https://doi.org/10.5194/egusphere-2025-53
Preprint. Discussion started: 24 January 2025

References

Amitai, Y., Ashkenazy, Y., and Gildor, H.: Multiple equilibria and overturning variability of the Aegean-Adriatic Seas, Global and Planetary Change, 151, 49–59, 2017.

Amitai, Y., Ashkenazy, Y., and Gildor, H.: The effect of wind-stress over the Eastern Mediterranean on deep-water formation in the Adriatic Sea, Deep Sea Research Part II: Topical Studies in Oceanography, 164, 5–13, 2019.

Ashkenazy, Y. and Gildor, H.: On the probability and spatial distribution of ocean surface currents, J. Phys. Oceanogr., 41, 2295–2306, 2011.

Ashkenazy, Y., Stone, P. H., and Malanotte-Rizzoli, P.: Box modeling of the Eastern Mediterranean sea, Physica A: Statistical Mechanics and its applications, 391, 1519–1531, 2012.

Ashkenazy, Y., Fredj, E., Gildor, H., Gong, G.-C., and Lee, H.-J.: Current temporal asymmetry and the role of tides: Nan-Wan Bay vs. the Gulf of Elat, Ocean Science, 12, 733–742, 2016.

Bauer, E.: Characteristic frequency distributions of remotely sensed in situ and modelled wind speeds, International Journal of Climatology, 16, 1087–1102, 1996.

Bel, G. and Ashkenazy, Y.: The relationship between the statistics of open ocean currents and the temporal correlations of the wind stress, New Journal of Physics, 15, 053 024, 2013.

Bergamasco, A. and Malanotte-Rizzoli, P.: The circulation of the Mediterranean Sea: a historical review of experimental investigations, Advances in Oceanography and Limnology., 1, 11–28, 2010.

Bowden, G., Barker, P., Shestopal, V., and Twidell, J.: The Weibull distribution function and wind power statistics, Wind Engineering, pp. 85–98, 1983.

Bracco, A., Lacasce, J., Pasquero, C., and Provenzale, A.: The velocity distribution of barotropic turbulence, Physics of Fluids, 12, 2478–2488, 2000a.

Bracco, A., LaCasce, J., and Provenzale, A.: Velocity probability density functions for oceanic floats, Journal of physical oceanography, 30, 461–474, 2000b.

Bracco, A., Chassignet, E. P., Garraffo, Z. D., and Provenzale, A.: Lagrangian velocity distributions in a high-resolution numerical simulation of the North Atlantic, J. Atmospheric and Oceanic Technology, 20, 1212–1220, 2003.

Campisi-Pinto, S., Gianchandani, K., and Ashkenazy, Y.: Statistical tests for the distribution of surface wind and current speeds across the globe, Renewable Energy, 149, 861–876, 2020.

Carta, J. and Ramirez, P.: Analysis of two-component mixture Weibull statistics for estimation of wind speed distributions, Renewable Energy, 32, 518–531, 2007.

Carta, J. A., Ramirez, P., and Velazquez, S.: A review of wind speed probability distributions used in wind energy analysis: Case studies in the Canary Islands, Renewable and sustainable energy reviews, 13, 933–955, 2009.

Chu, P. C.: Probability distribution function of the upper equatorial Pacific current speeds, Geophys. Res. Lett., 35, L12 606, 2008a.

Chu, P. C.: Weibull Distribution for the Global Surface Current Speeds Obtained from Satellite Altimetry, in: Geoscience and Remote Sensing Symposium, 2008. IGARSS 2008. IEEE International, vol. 3, pp. III–59, IEEE, 2008b.

Chu, P. C.: Statistical Characteristics of the Global Surface Current Speeds Obtained From Satellite Altimetry and Scatterometer Data, IEEE J. of Selected Topics in Applied Earth Observations and Remote Sensing, 2, 27–32, 2009.

Conradsen, K., Nielsen, L., and Prahm, L.: Review of Weibull statistics for estimation of wind speed distributions, Journal of climate and Applied Meteorology, 23, 1173–1183, 1984.

https://doi.org/10.5194/egusphere-2025-53
Preprint. Discussion started: 24 January 2025

Davidson, R., MacKinnon, J. G., et al.: Econometric theory and methods, vol. 5, Oxford University Press New York, 2004.

Debreu, L., Marchesiello, P., Penven, P., and Cambon, G.: Two-way nesting in split-explicit ocean models: Algorithms, implementation and validation, Ocean Modelling, 49, 1–21, 2012.

Drobinski, P., Coulais, C., and Jourdier, B.: Surface wind-speed statistics modelling: alternatives to the Weibull distribution and performance evaluation, Boundary-Layer Meteorology, 157, 97–123, 2015.

Ekman, V. W.: On the influence of the earth's rotation in ocean-currents, Arch. Math. Astron. Phys., 2, 1–52, 1905.

Escudier, R., Clementi, E., Omar, M., Cipollone, A., Pistoia, J., Aydogdu, A., Drudi, M., Grandi, A., Lyubartsev, V., Lecci, R., et al.: Mediterranean Sea Physical reanalysis (CMEMS MED-currents)(version 1)[Data set], Copernicus Monitoring Environment Marine Service (CMEMS), 2020.

Feliks, Y., Gildor, H., and Mantel, N.: Intraseasonal oscillatory modes in the eastern Mediterranean Sea, Journal of Physical Oceanography, 52, 1471–1482, 2022.

Ferguson, J., Henderson, G., Kucera, M., and Rickaby, R.: Systematic change of foraminiferal Mg/Ca ratios across a strong salinity gradient, Earth and Planetary Science Letters, 265, 153–166, 2008.

Gille, S. T. and Smith, S. G. L.: Velocity probability density functions from altimetry, J. Phys. Oceanogr., 30, 125–136, 2000.

Haim, N., Grigorieva, V., Toledo, Y., Soffer, R., Mayzel, B., Katz, T., Alkalay, R., Biton, E., Lazar, A., Gildor, H., et al.: Multiyear surface waves dataset from the subsurface "DeepLev" Eastern Levantine moored station, Earth System Science Data Discussions, 2023, 1–16, 2023.

Justus, C., Hargraves, W., Mikhail, A., and Graber, D.: Methods for estimating wind speed frequency distributions, Journal of applied meteorology, 17, 350–353, 1978.

Kabir, A., Lemongo-Tchamba, I., and Fernandez, A.: An assessment of available ocean current hydrokinetic energy near the North Carolina shore, Renewable energy, 80, 301–307, 2015.

Katz, T., Weinstein, Y., Alkalay, R., Biton, E., Toledo, Y., Lazar, A., Zlatkin, O., Soffer, R., Rahav, E., Sisma-Ventura, G., et al.: The first deep-sea mooring station in the eastern Levantine basin (DeepLev), outline and insights into regional sedimentological processes, Deep Sea Research Part II: Topical Studies in Oceanography, 171, 104 663, 2020.

Kelly, M., Troen, I., and Jørgensen, H. E.: Weibull-k revisited: "tall" profiles and height variation of wind statistics, Boundary-layer meteorology, 152, 107–124, 2014.

Kiss, P. and Jánosi, I. M.: Comprehensive empirical analysis of ERA-40 surface wind speed distribution over Europe, Energy Conversion and Management, 49, 2142–2151, 2008.

Laws, K., Paduan, J. D., and Vesecky, J.: Estimation and Assessment of Errors Related to Antenna Pattern Distortion in CODAR SeaSonde High-Frequency Radar Ocean Current Measurements, J. Oceanic and Atmos. Tech., 27, 1029—1043, 2010.

Lun, I. Y. and Lam, J. C.: A study of Weibull parameters using long-term wind observations, Renewable Energy, 20, 145–153, 2000.

Malanotte-Rizzoli, P., Artale, V., Borzelli-Eusebi, G., Brenner, S., Crise, A., Gacic, M., Kress, N., Marullo, S., Ribera d'Alcalà, M., Sofianos, S., et al.: Physical forcing and physical/biochemical variability of the Mediterranean Sea: a review of unresolved issues and directions for future research, Ocean Science, 10, 281–322, 2014.

Mantel, N., Feliks, Y., Gildor, H., Poulain, P.-M., Mauri, E., and Menna, M.: Seasonal and vertical tidal variability in the Southeastern Mediterranean Sea, Frontiers in Marine Science, 11, 1388 137, 2024.

Manwell, J. F., McGowan, J. G., and Rogers, A. L.: Wind energy explained: theory, design and application, John Wiley & Sons, 2010.

https://doi.org/10.5194/egusphere-2025-53
Preprint. Discussion started: 24 January 2025

Mavropoulou, A.-M., Vervatis, V., and Sofianos, S.: The Mediterranean Sea overturning circulation: A hindcast simulation (1958–2015) with an eddy-resolving (1/36) model, Deep Sea Research Part I: Oceanographic Research Papers, 187, 103 846, 2022.

Monahan, A. H.: The Probability Distribution of Sea Surface Wind Speeds. Part I: Theory and SeaWinds Observations, J. Climate, 19, 497–520, 2006a.

Monahan, A. H.: The probability distribution of sea surface wind speeds. Part II: Dataset intercomparison and seasonal variability, Journal of Climate, 19, 521–534, 2006b.

Morrissey, M. L. and Greene, J. S.: Tractable analytic expressions for the wind speed probability density functions using expansions of orthogonal polynomials, Journal of Applied Meteorology and Climatology, 51, 1310–1320, 2012.

Munk, W. H.: On the wind-driven ocean circulation, Journal of Atmospheric Sciences, 7, 80–93, 1950.

Paquette, R. G.: Some statistical properties of ocean currents, Ocean Engineering, 2, 95–114, 1972.

Parras-Berrocal, I. M., Vázquez, R., Cabos, W., Sein, D. V., Álvarez, O., Bruno, M., and Izquierdo, A.: Surface and intermediate water changes triggering the future collapse of deep water formation in the North Western Mediterranean, Geophysical Research Letters, 49, e2021GL095 404, 2022.

Parras-Berrocal, I. M., Vazquez, R., Cabos, W., Sein, D. V., Álvarez, O., Bruno, M., and Izquierdo, A.: Dense water formation in the Eastern Mediterranean under global warming scenario, EGUsphere, pp. 1–17, 2023.

Pinardi, N., Estournel, C., Cessi, P., Escudier, R., and Lyubartsev, V.: Dense and deep water formation processes and Mediterranean overturning circulation, in: Oceanography of the Mediterranean Sea, pp. 209–261, Elsevier, 2023.

Roether, W., Manca, B., Klein, B., Bregant, D., Georgopoulos, D., Beitzel, V., Kovacevic, V., and Luchetta, A.: Recent changes in Eastern Mediterranean deep waters, Science, 271, 333–335, 1996.

Seguro, J. and Lambert, T.: Modern estimation of the parameters of the Weibull wind speed distribution for wind energy analysis, Journal of Wind Engineering and Industrial Aerodynamics, 85, 75–84, 2000.

Shaltout, M. and Omstedt, A.: Recent sea surface temperature trends and future scenarios for the Mediterranean Sea, Oceanologia, 56, 411–443, 2014.

Shchepetkin, A. F. and McWilliams, J. C.: The Regional Ocean Modeling System (ROMS): A split-explicit, free- surface, topography-following coordinates ocean model, Ocean Modell., 9, 347–404, 2005.

Smith, S. G. L. and Gille, S. T.: Probability density functions of large-scale turbulence in the ocean, Phys. Rev. Lett., 81, 5249, 1998.

Solodoch, A., Barkan, R., Verma, V., Gildor, H., Toledo, Y., Khain, P., and Levi, Y.: Basin-Scale to Submesoscale Variability of the East Mediterranean Sea Upper Circulation, Journal of Physical Oceanography, 53, 2137–2158, 2023.

Stommel, H.: The westward intensification of wind-driven ocean currents, Eos, Transactions American Geophysical Union, 29, 202–206, 1948.

Stommel, H. and Arons, A. B.: On the abyssal circulation of the world ocean - I. Stationary planetary flow patterns on a sphere, Deep Sea Res., 6, 140–154, 1960.

Takle, E. S. and Brown, J.: Note on the use of Weibull statistics to characterize wind-speed data, Journal of applied meteorology, 17, 556–559, 1978.

Tanhua, T., Hainbucher, D., Cardin, V., Álvarez, M., Civitarese, G., McNichol, A., and Key, R.: Repeat hydrography in the Mediterranean Sea, data from the Meteor cruise 84/3 in 2011, Earth System Science Data, 5, 289–294, 2013.

Troen, I. and Petersen, E. L.: European wind atlas, Risø National Laboratory, 1989.

https://doi.org/10.5194/egusphere-2025-53
Preprint. Discussion started: 24 January 2025

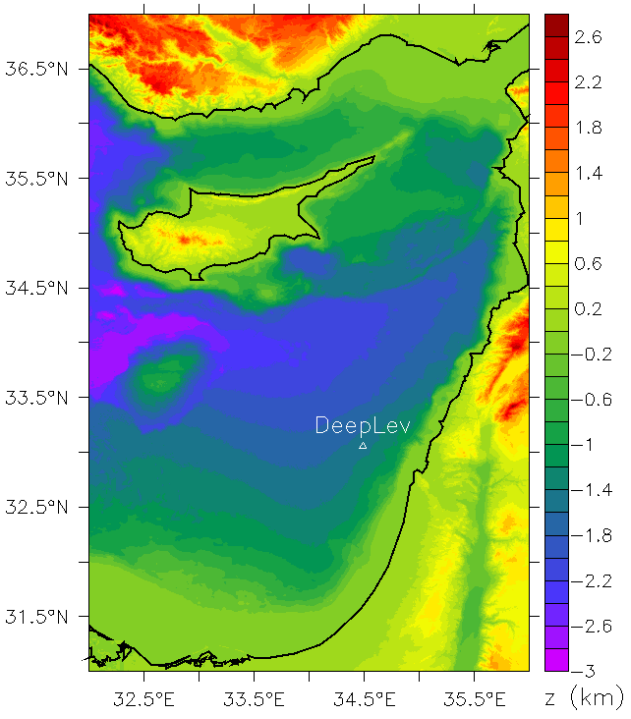

Figure 1. Bathymetric map of Israeli waters and the greater Levant region. The location of the DeepLev station is indicated by the white triangle. The black contour line indicates the coastline.

Tuller, S. E. and Brett, A. C.: The characteristics of wind velocity that favor the fitting of a Weibull distribution in wind speed analysis, Journal of Climate and Applied Meteorology, 23, 124–134, 1984.

Ulgen, K. and Hepbasli, A.: Determination of Weibull parameters for wind energy analysis of Izmir, Turkey, International Journal of Energy Research, 26, 495–506, 2002.

https://doi.org/10.5194/egusphere-2025-53
Preprint. Discussion started: 24 January 2025

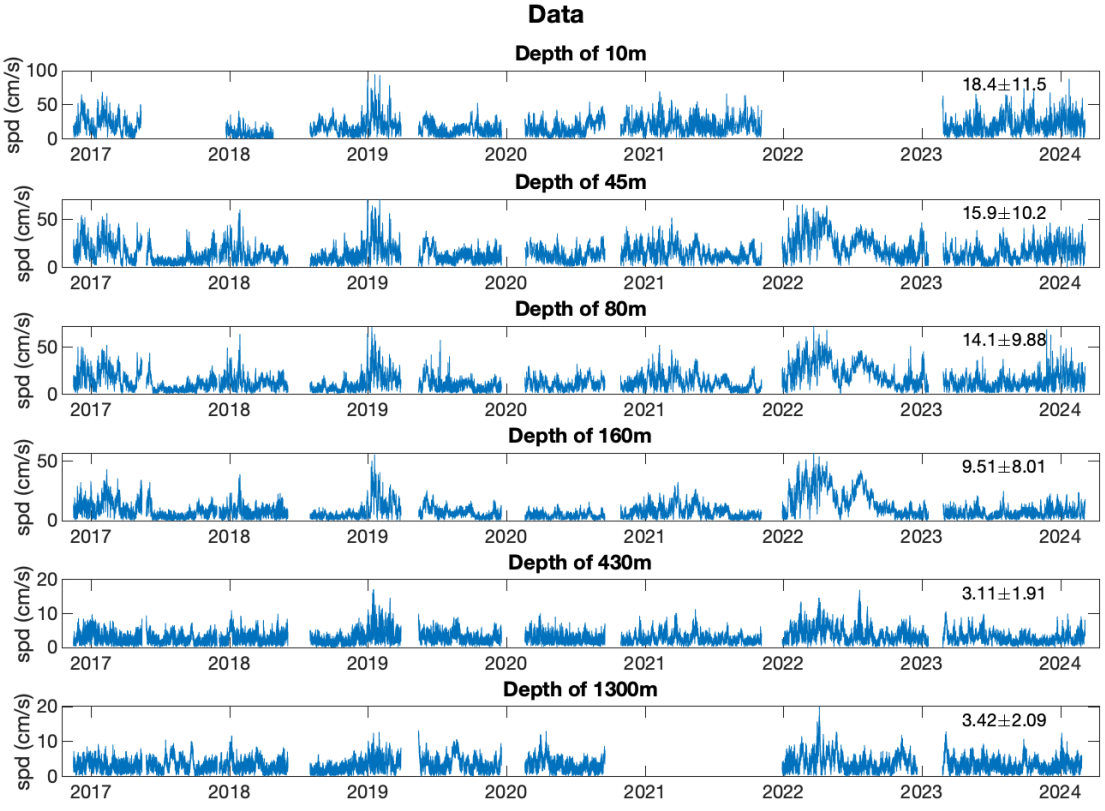

Figure 2. The measured current speed (in cm/s) time series for the different depths analyzed here. The numbers at the top right corner of each panel indicate the mean ± std. Note that the ordinate axes have different ranges in different panels.

https://doi.org/10.5194/egusphere-2025-53
Preprint. Discussion started: 24 January 2025

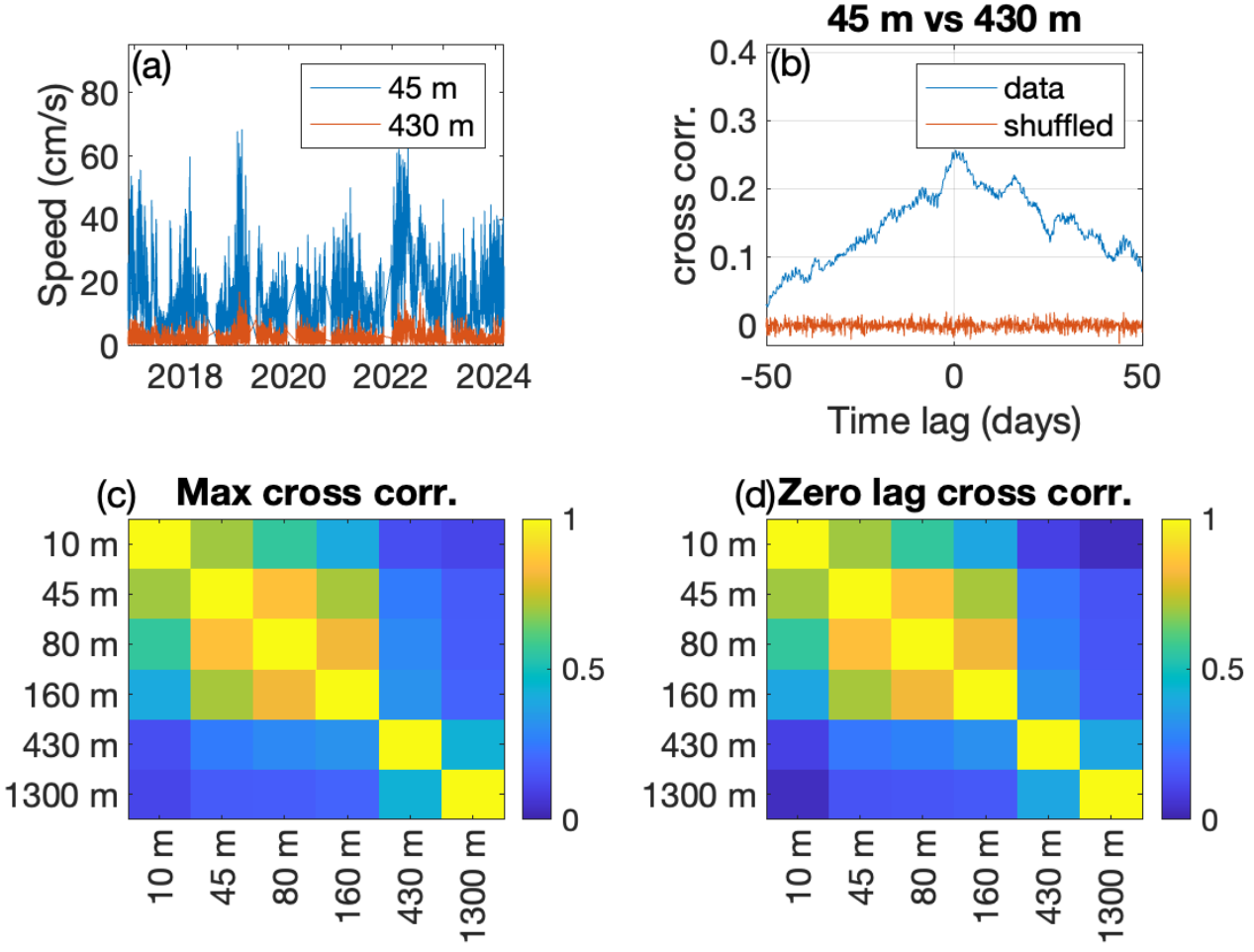

Figure 3. (a) The current time series of 45 m (blue) and 430 m (red) as a function of time. (b) The cross-correlation function between the two time series shown in a (blue) as a function of time lag (in days). The red time series depicts the time cross-correlation of the shuffled time series (red). (c) The maximum cross-correlation between the time series of the different depths. (d) The zero-lag cross-correlation between the time series of the different depths. Note the similarity to panel c.

https://doi.org/10.5194/egusphere-2025-53
Preprint. Discussion started: 24 January 2025

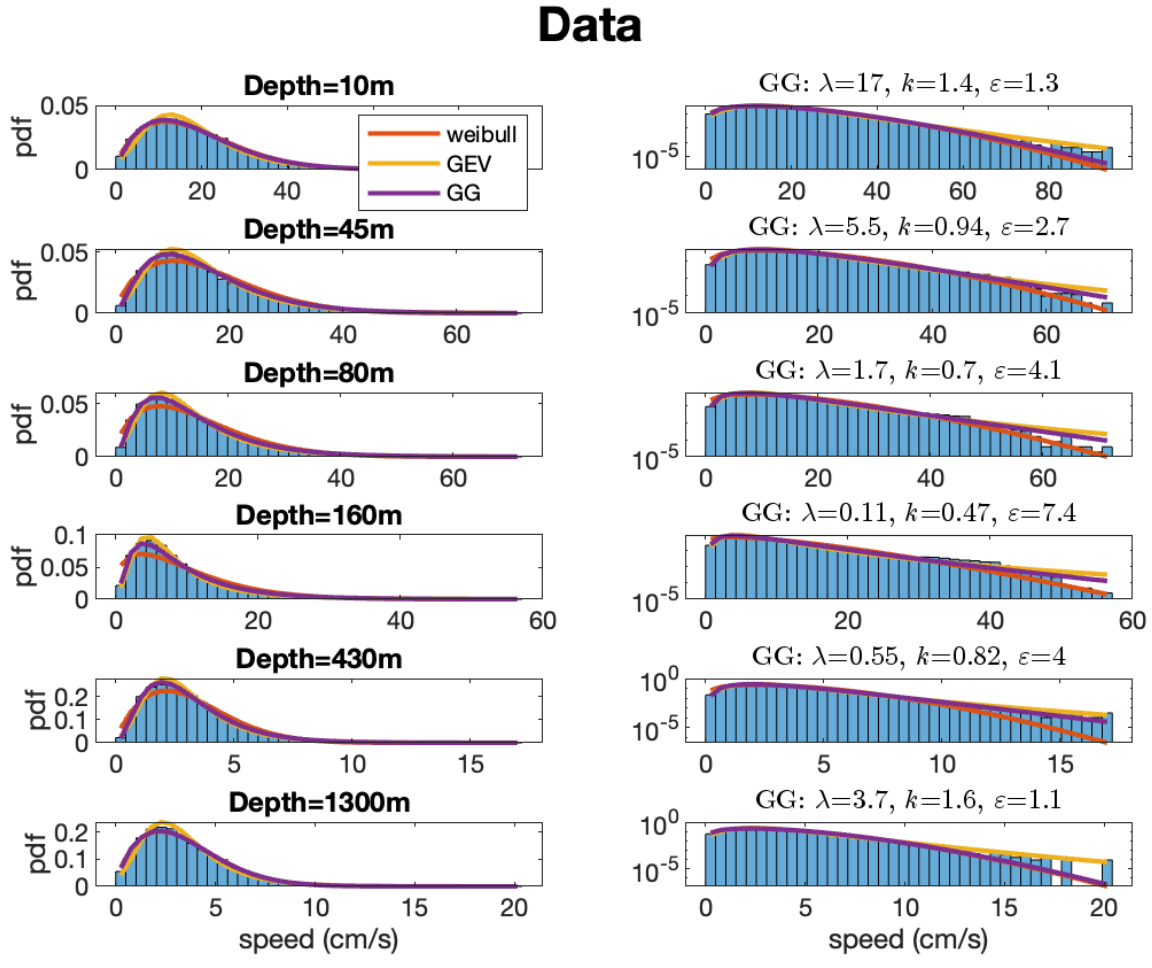

Figure 4. The pdfs of the current speed time series shown in Fig. 2 in regular (left panels) and semi-log (right panels) plots. The corresponding depths are indicated in the title of the left panels whereas the parameters of the fitted generalized gamma (GG) pdf are indicated in the title of the right panels. The fitted Weibull (red), GEV (yellow), and GG (purple) pdfs are also included.

https://doi.org/10.5194/egusphere-2025-53
Preprint. Discussion started: 24 January 2025

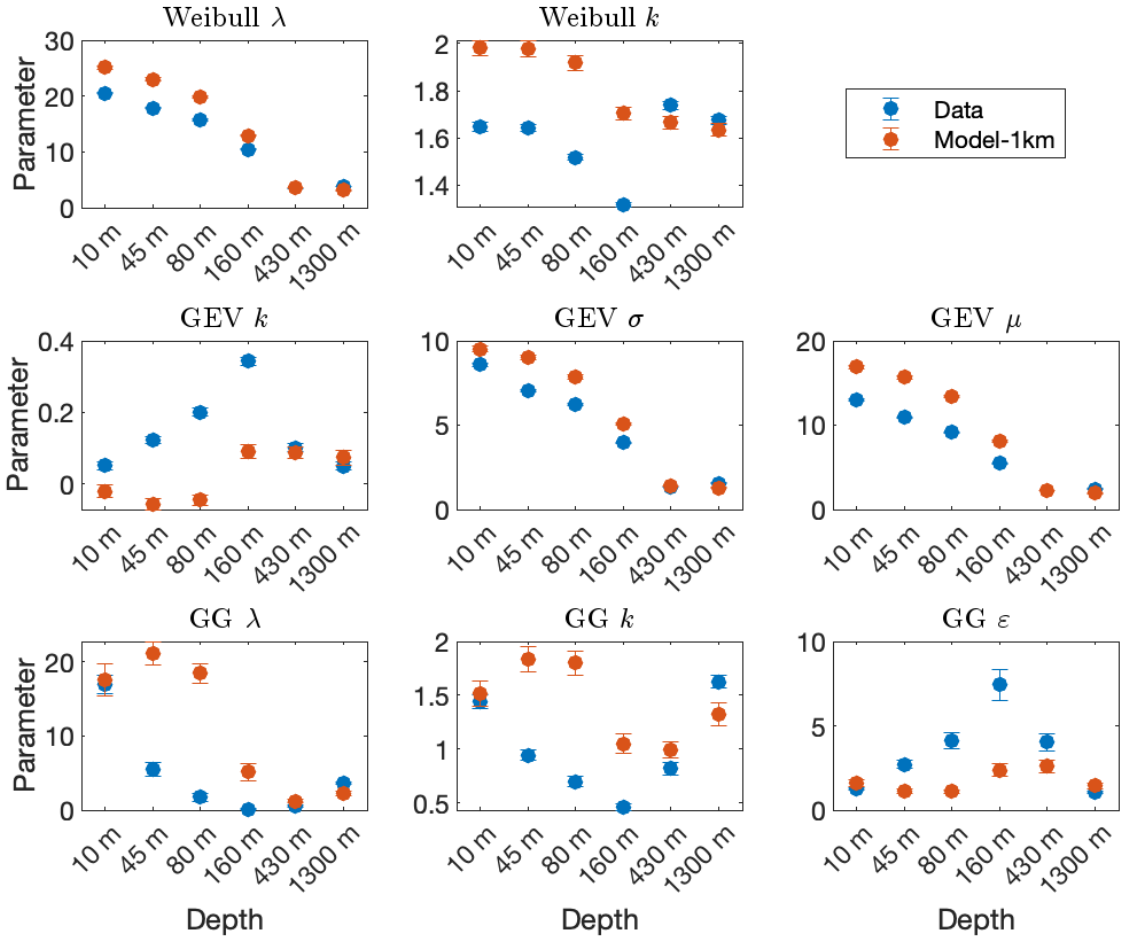

Figure 5. The estimated pdf parameters versus depth of the: data (blue circles) and 1 km resolution model (red circles), for the: Weibull (upper panels), GEV (middle panels), and GG (lower panels) distributions. The error bars indicate the 5-95% confidence interval (which is not always visible). The estimated GG parameters for the data at depths of 80 m and 160 m (represented by the blue circles in the bottom panels) are less accurate as the MLE did not converge.

https://doi.org/10.5194/egusphere-2025-53
Preprint. Discussion started: 24 January 2025

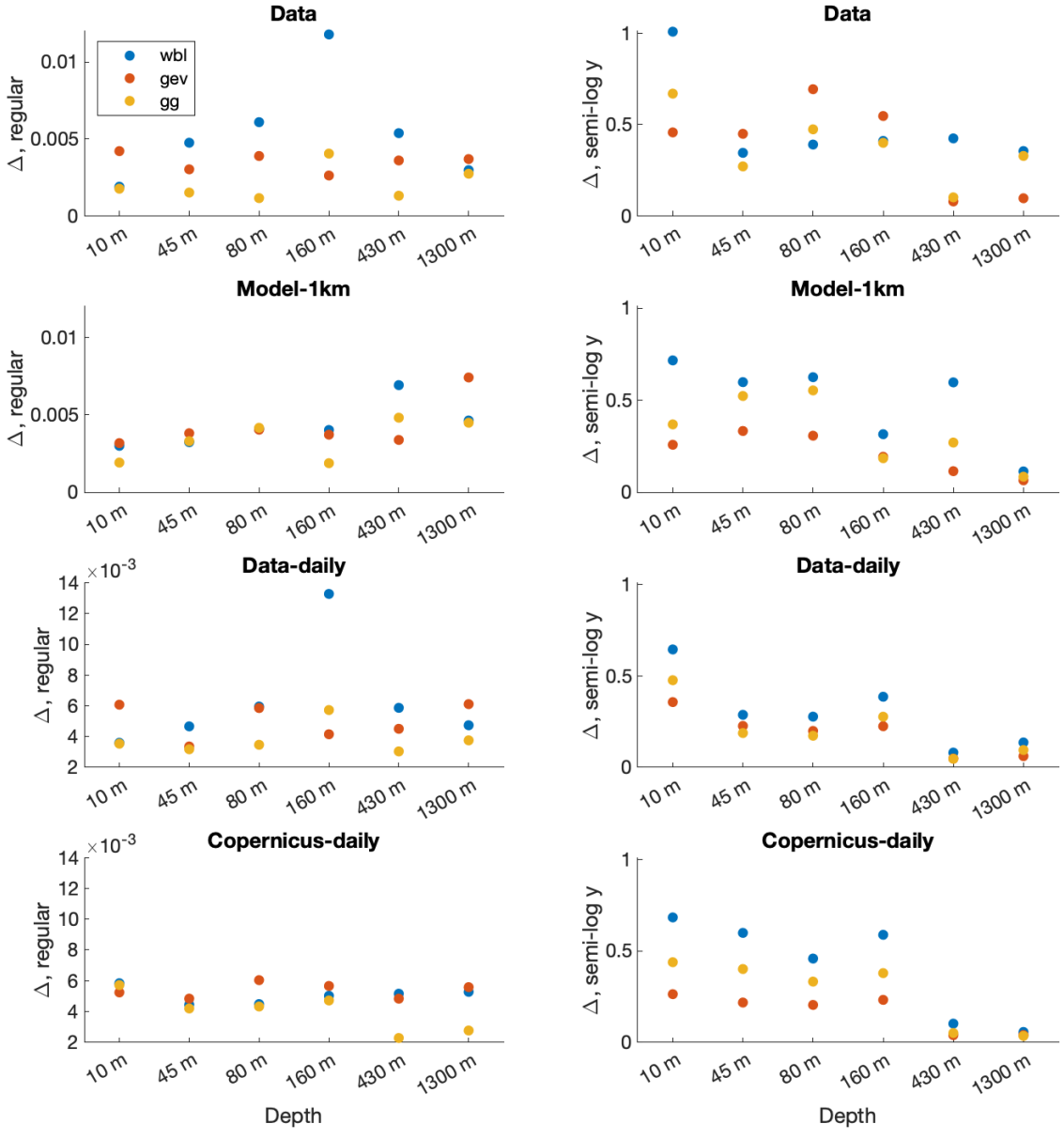

Figure 6. The depth dependence of the difference measure Δ, i.e., the difference between the observed and fitted distributions for the measured data (upper panels), 1 km resolution model (second-row panels), daily mean measured currents (third-row panels), and Copernicus daily mean reanalysis (bottom panels). Presented are the results for the fit to the Weibull (WBL, blue), GEV (red), and GG (yellow) distributions, calculated based on regular (left panels) and semi-log (right panels) pdfs.

https://doi.org/10.5194/egusphere-2025-53
Preprint. Discussion started: 24 January 2025

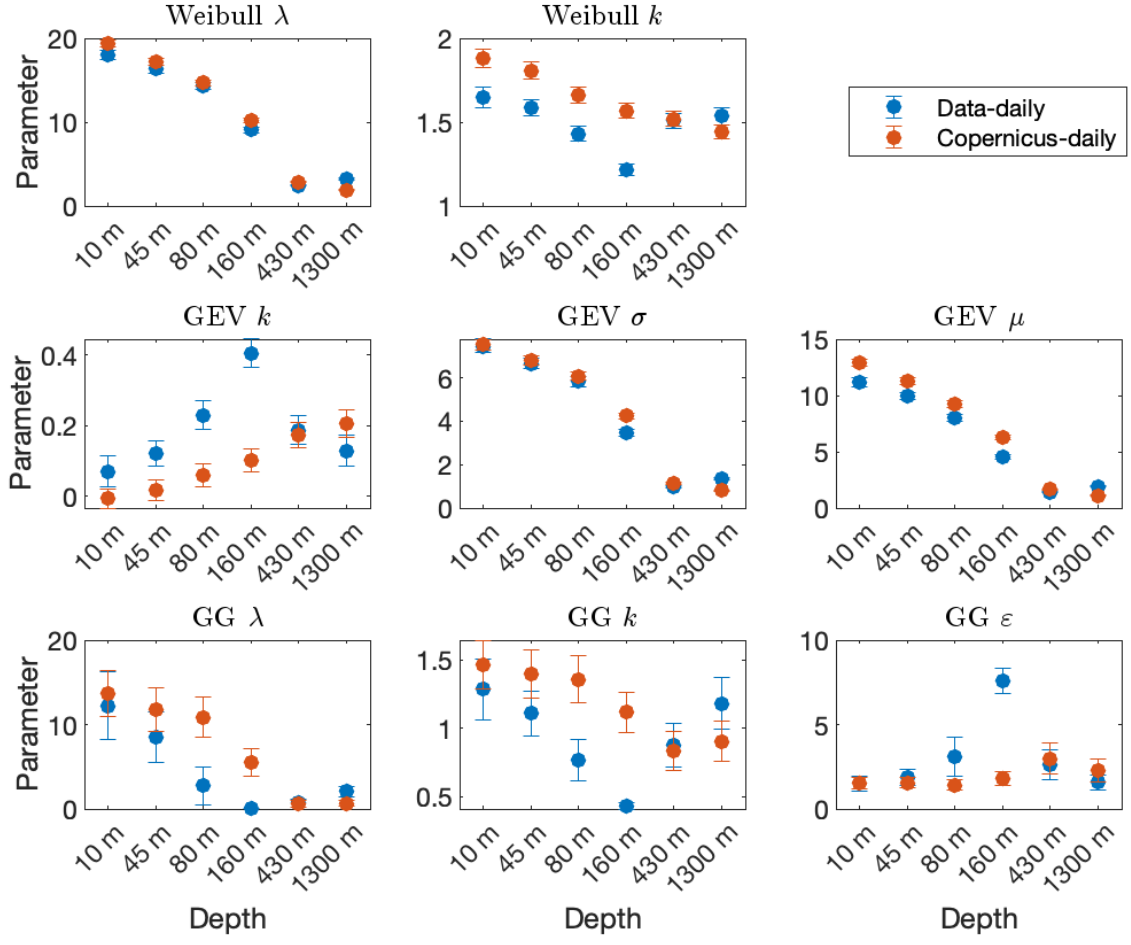

Figure 7. Same as Fig. 5 for the daily mean current speed of the data (blue circles) and 1 km resolution daily mean Copernicus model data.

https://doi.org/10.5194/egusphere-2025-53
Preprint. Discussion started: 24 January 2025

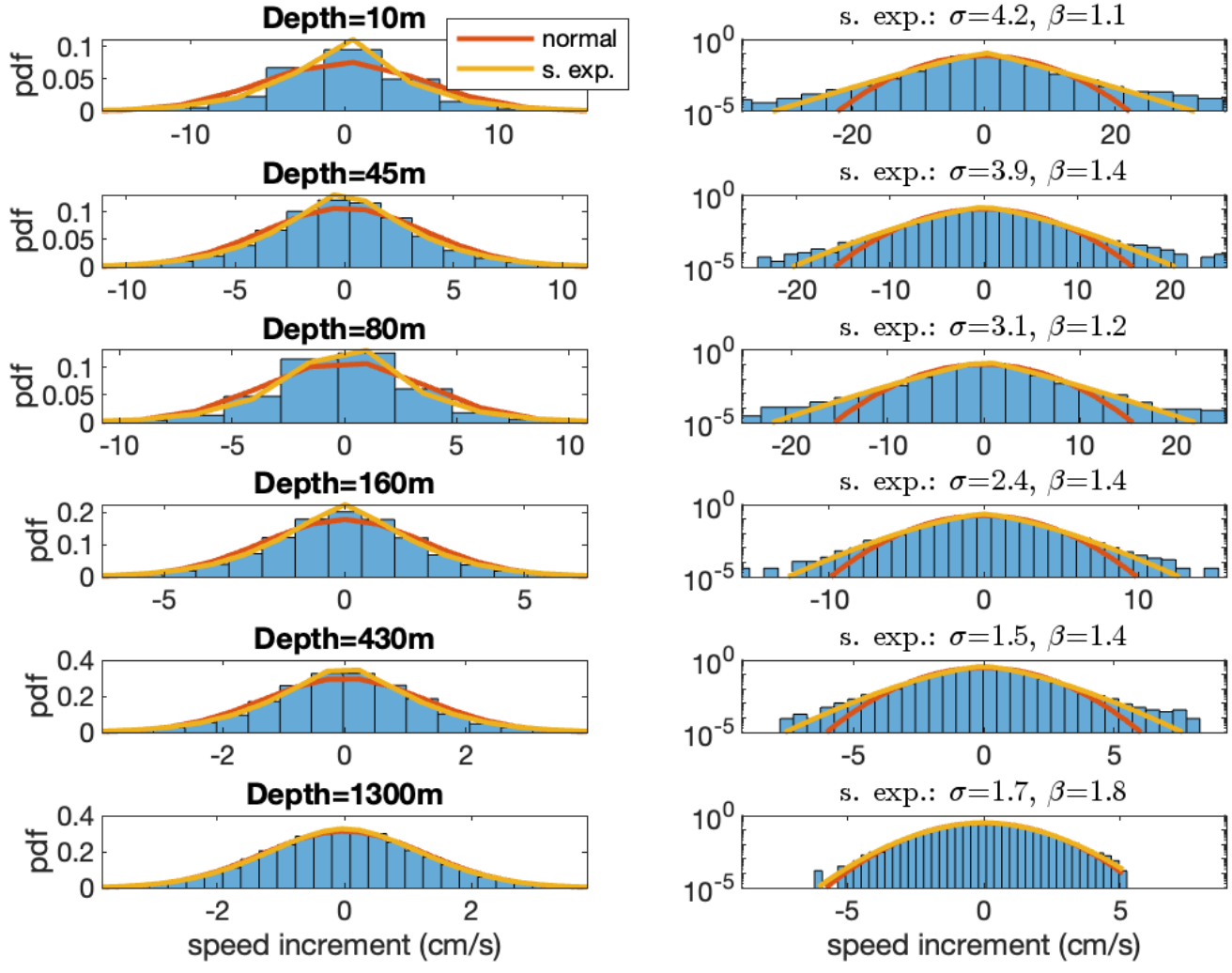

Figure 8. The pdfs of the current speed increment time series in regular (left panels) and semi-log (right panels) plots. The corresponding depths are indicated in the title of the left panels whereas the parameters of the fitted stretched exponential distribution are indicated in the title of the right panels. The fitted normal (red) and stretched exponential (yellow) are also included.

https://doi.org/10.5194/egusphere-2025-53
Preprint. Discussion started: 24 January 2025

Appendix A

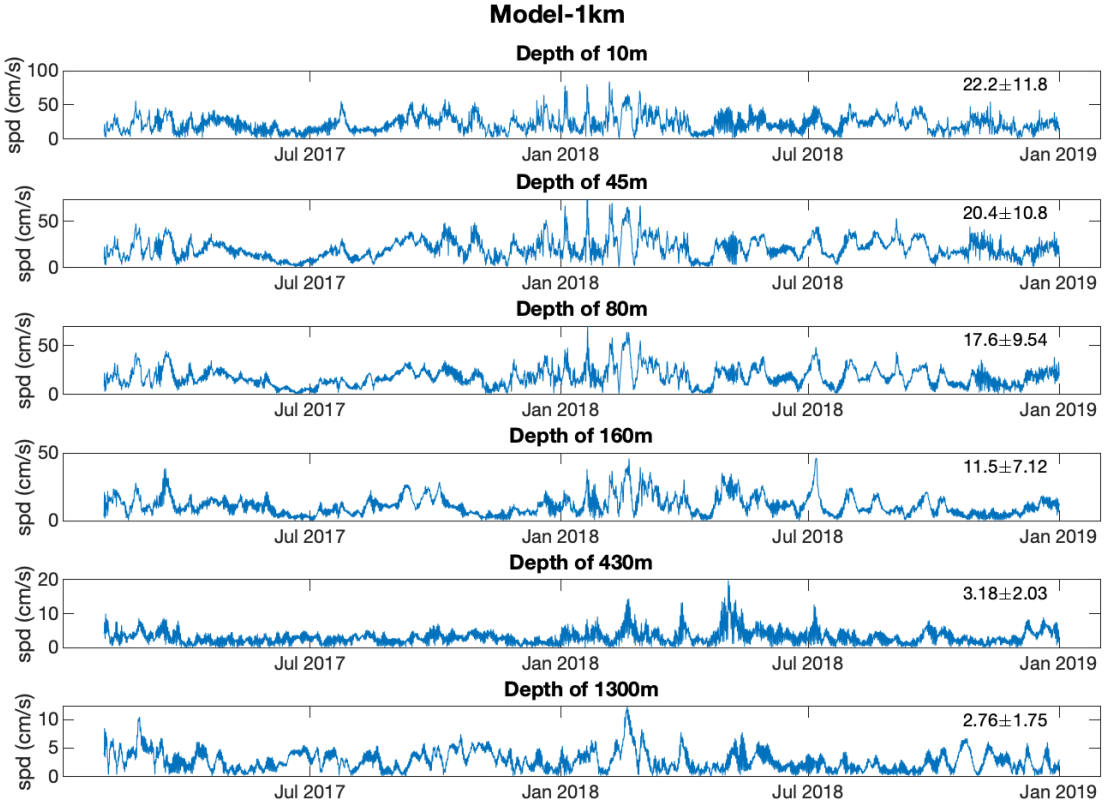

Figure A1. The model (1 km resolution) current speed (in cm/s) time series for different depths. The numbers on the top right of each panel indicate the mean ± std of the current time series.

https://doi.org/10.5194/egusphere-2025-53
Preprint. Discussion started: 24 January 2025

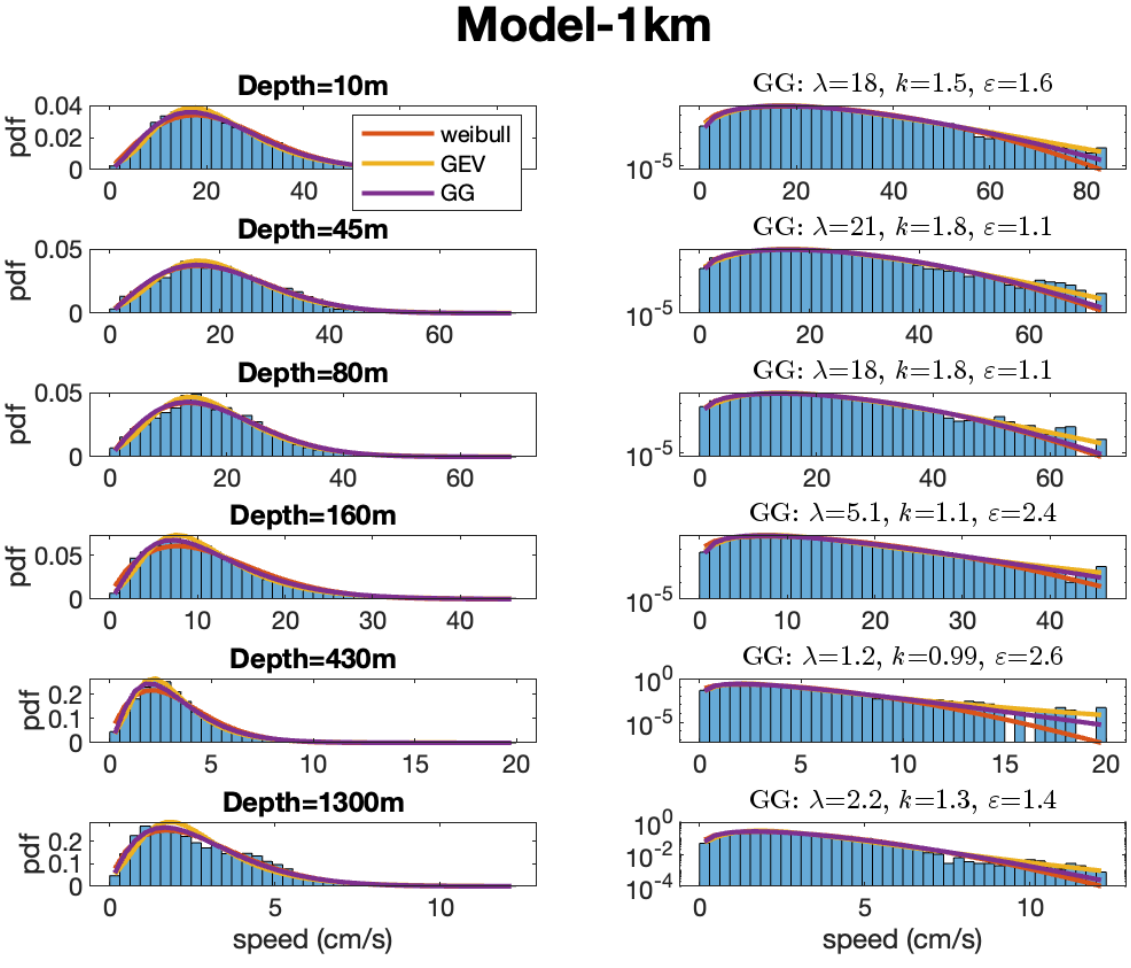

Figure A2. The pdfs of the (1 km resolution) model's current speed time series shown in Fig. A1 in regular (left panels) and semi-log (right panels) plots. The corresponding depths are indicated in the title of the left panels while the parameters of the fitted generalized gamma (GG) distribution are indicated in the title of the right panels. The fitted Weibull (red), GEV (yellow), and GG (purple) pdfs are also included.

https://doi.org/10.5194/egusphere-2025-53
Preprint. Discussion started: 24 January 2025

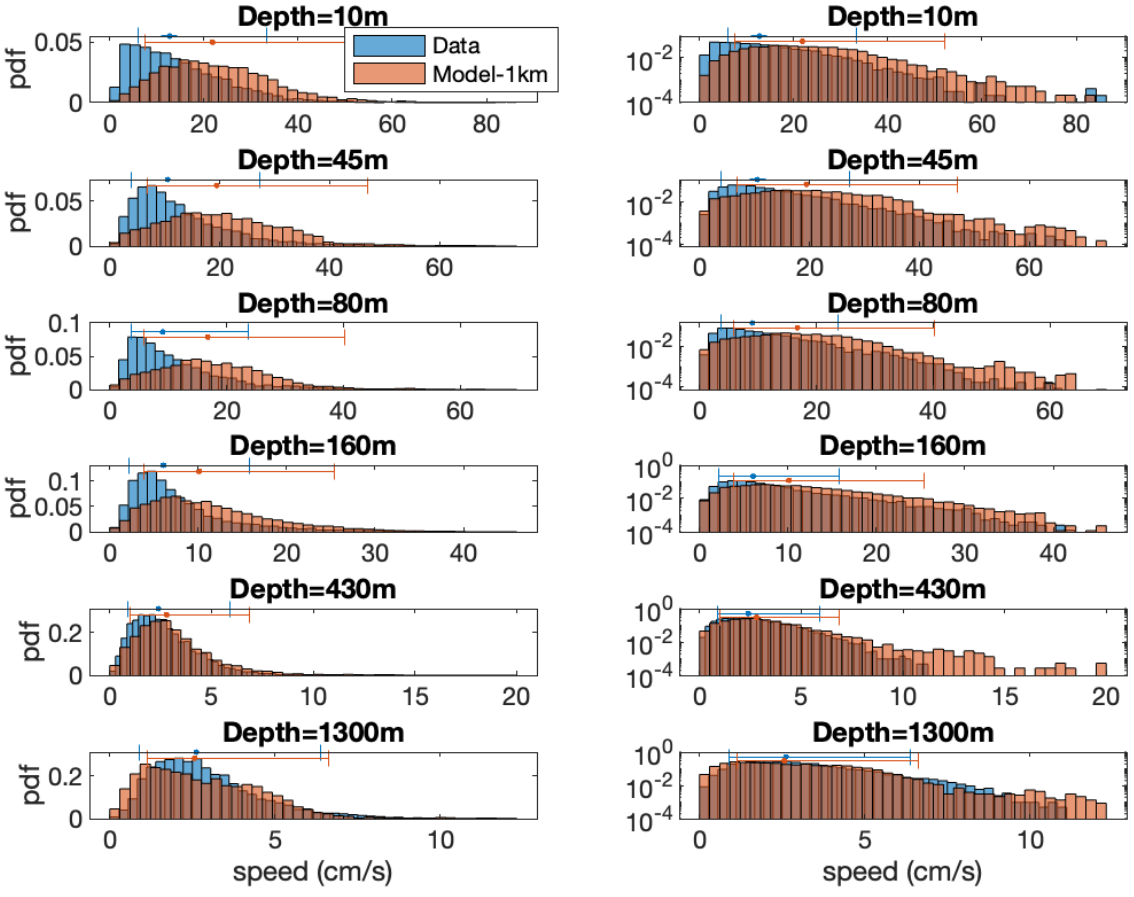

Figure A3. The data (blue) and model (light brown) pdfs of the current speed (two-hour resolution) in regular (left panels) and semi-log (right panels) plots, for time series of the common times of the data and model. The corresponding depths are indicated in the title of the panels. The overlapping part of the pdfs is indicated by the dark brown color, suggesting that model pdfs are stretched to the right, almost for all depths.

https://doi.org/10.5194/egusphere-2025-53
Preprint. Discussion started: 24 January 2025

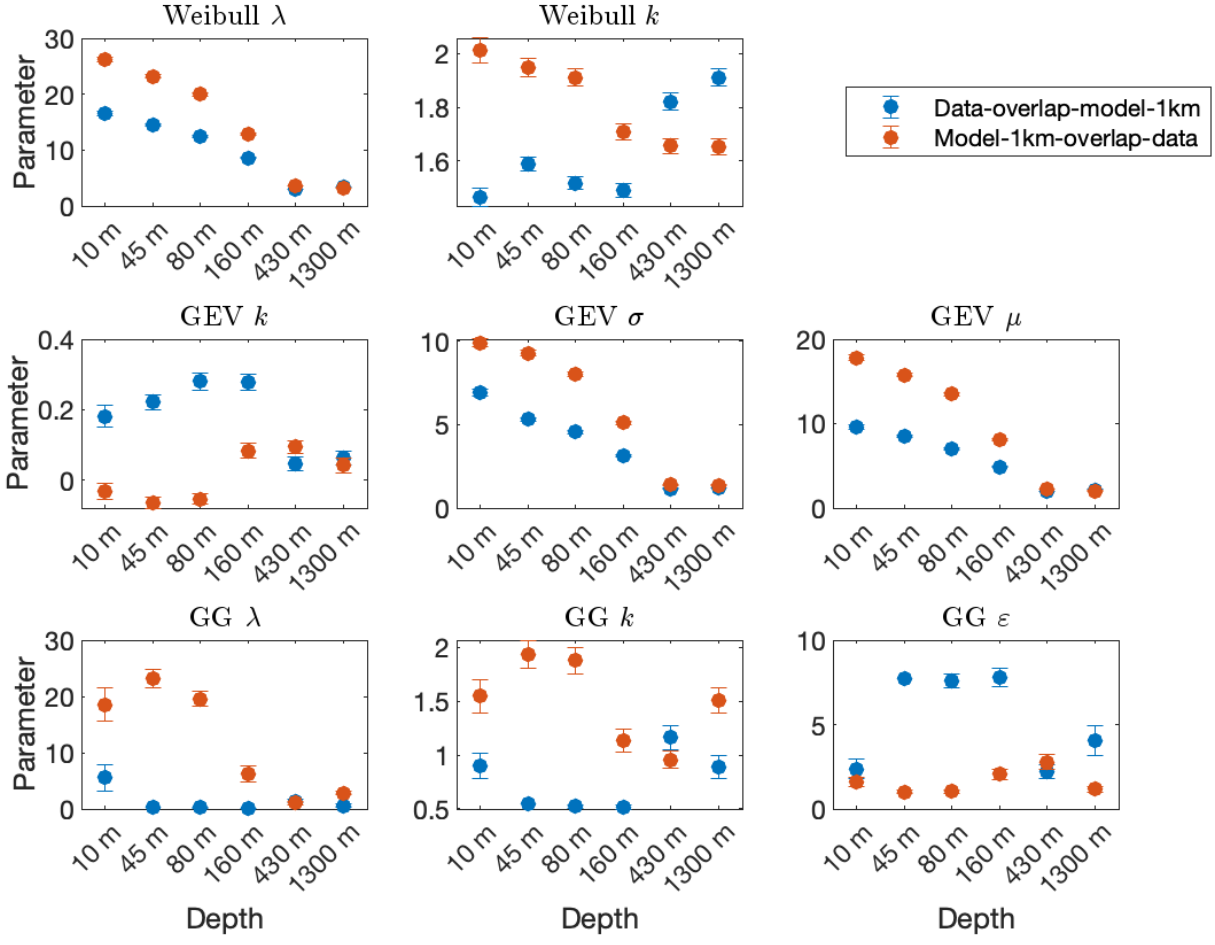

Figure A4. Same as Fig. 5 when using the data of the common times of the data and 1 km resolution model.

https://doi.org/10.5194/egusphere-2025-53
Preprint. Discussion started: 24 January 2025

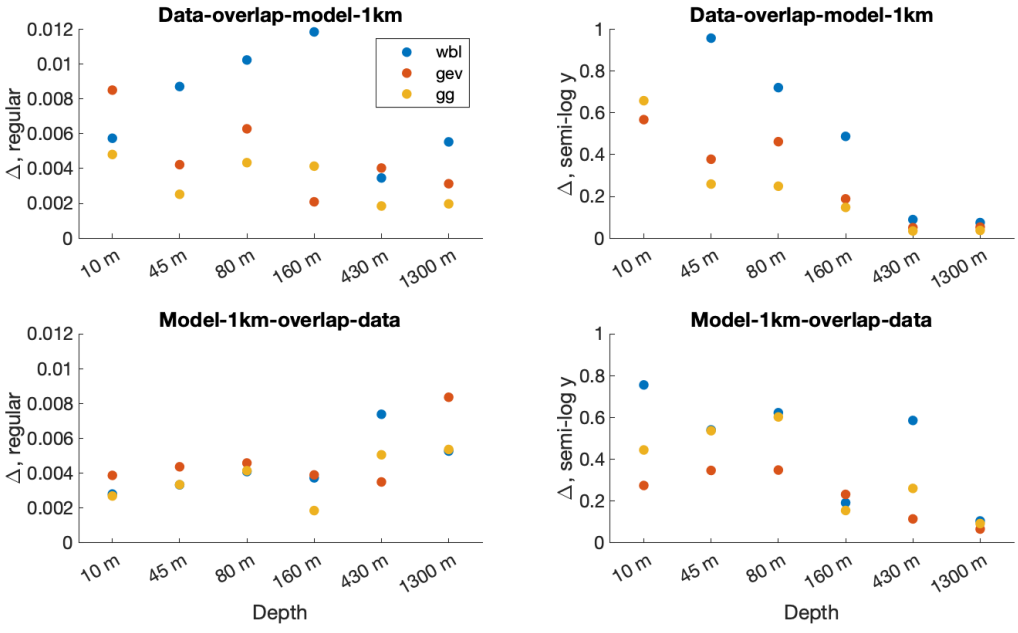

Figure A5. Same as the upper four panels of Fig. 6 for the data and model time series that share the same times.

https://doi.org/10.5194/egusphere-2025-53
Preprint. Discussion started: 24 January 2025

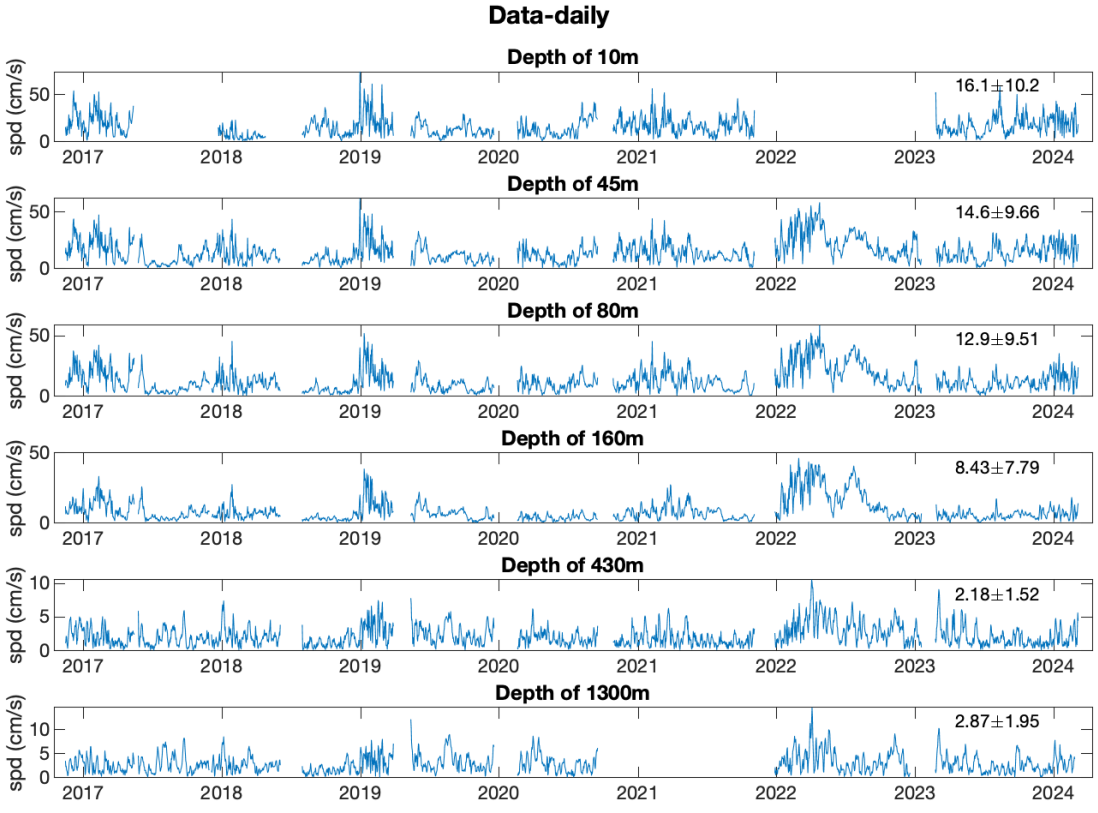

Figure A6. The data daily mean current speed (in cm/s) time series for different depths. The numbers on the top right of each panel indicate the mean ± std of the current time series.

https://doi.org/10.5194/egusphere-2025-53
Preprint. Discussion started: 24 January 2025

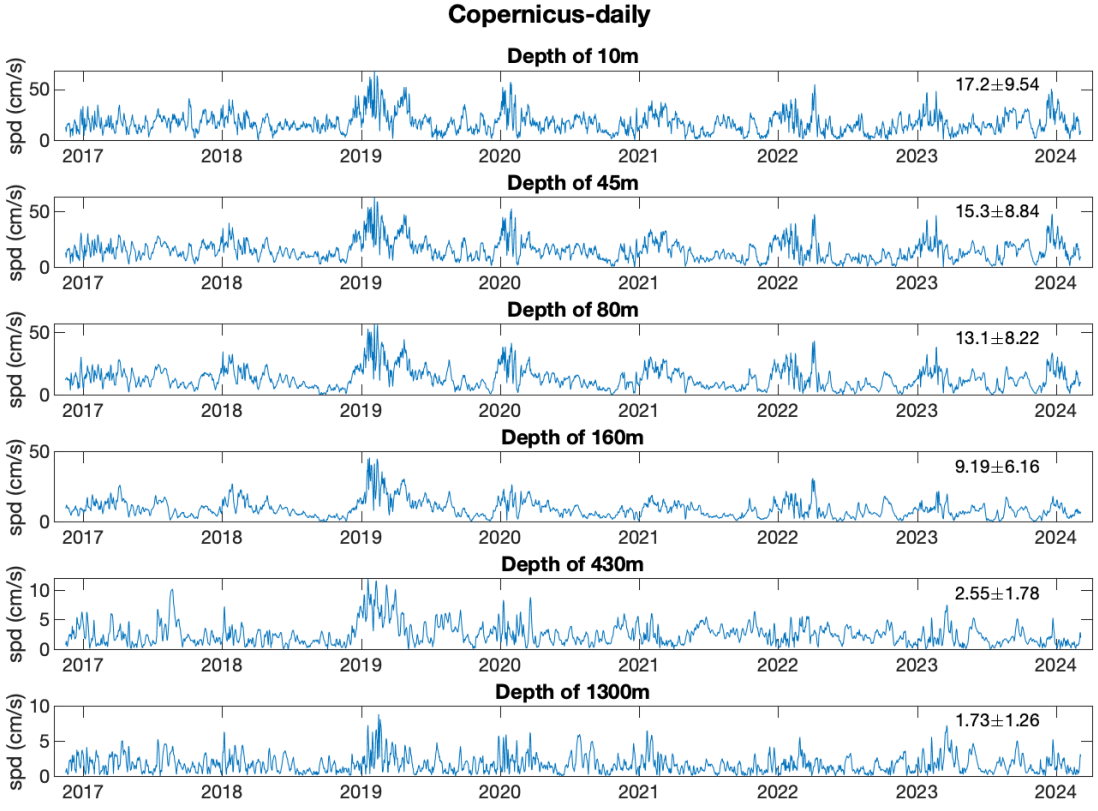

Figure A7. The Copernicus reanalysis daily mean current speed (in cm/s) time series (Escudier et al., 2020) for different depths. The numbers on the top right of each panel indicate the mean ± std of the current time series.

https://doi.org/10.5194/egusphere-2025-53
Preprint. Discussion started: 24 January 2025

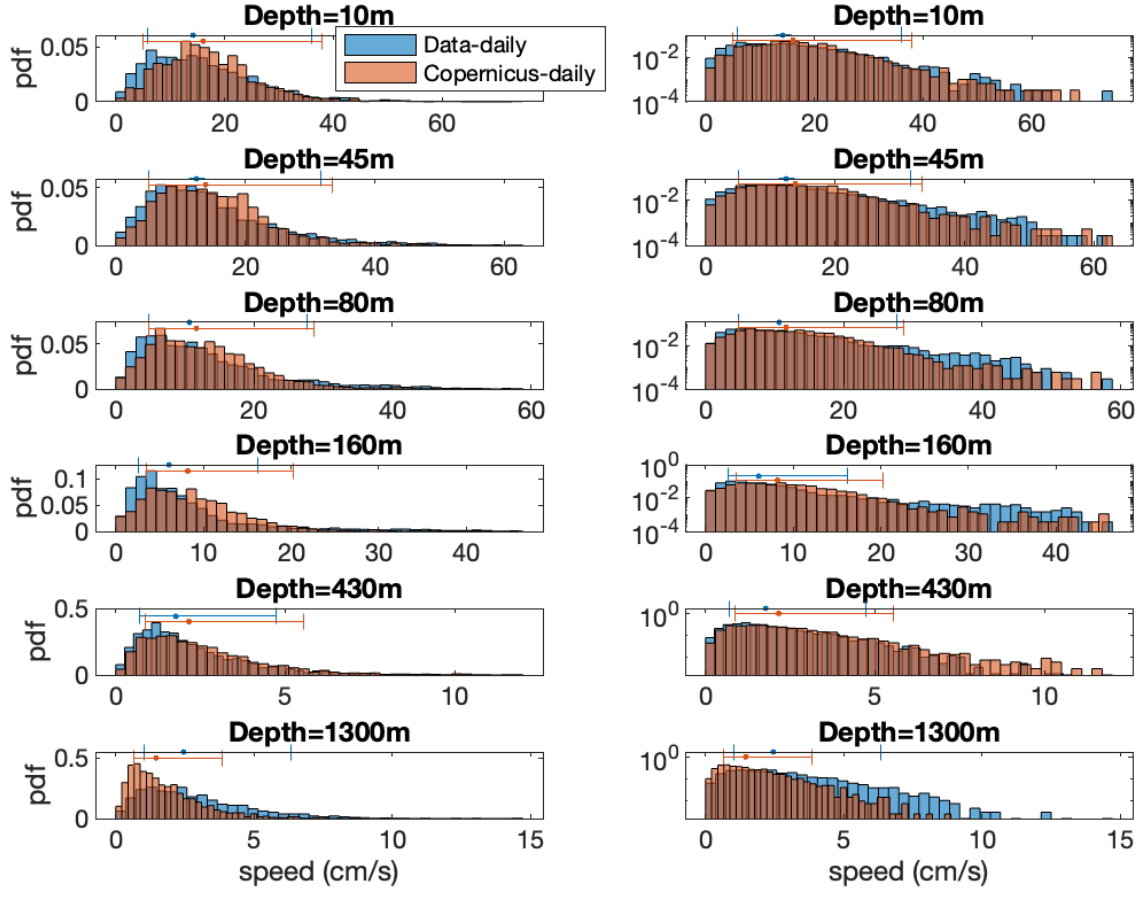

Figure A8. The data (blue) and Copernicus model (light brown) pdfs of the current speed (daily mean) in regular (left panels) and semi-log (right panels) plots. The corresponding depths are indicated in the title of the panels. The overlapping part of the pdfs is indicated by the dark brown color. The blue and light brown error bars indicate the median and 25%-75% quantiles.

https://doi.org/10.5194/egusphere-2025-53
Preprint. Discussion started: 24 January 2025

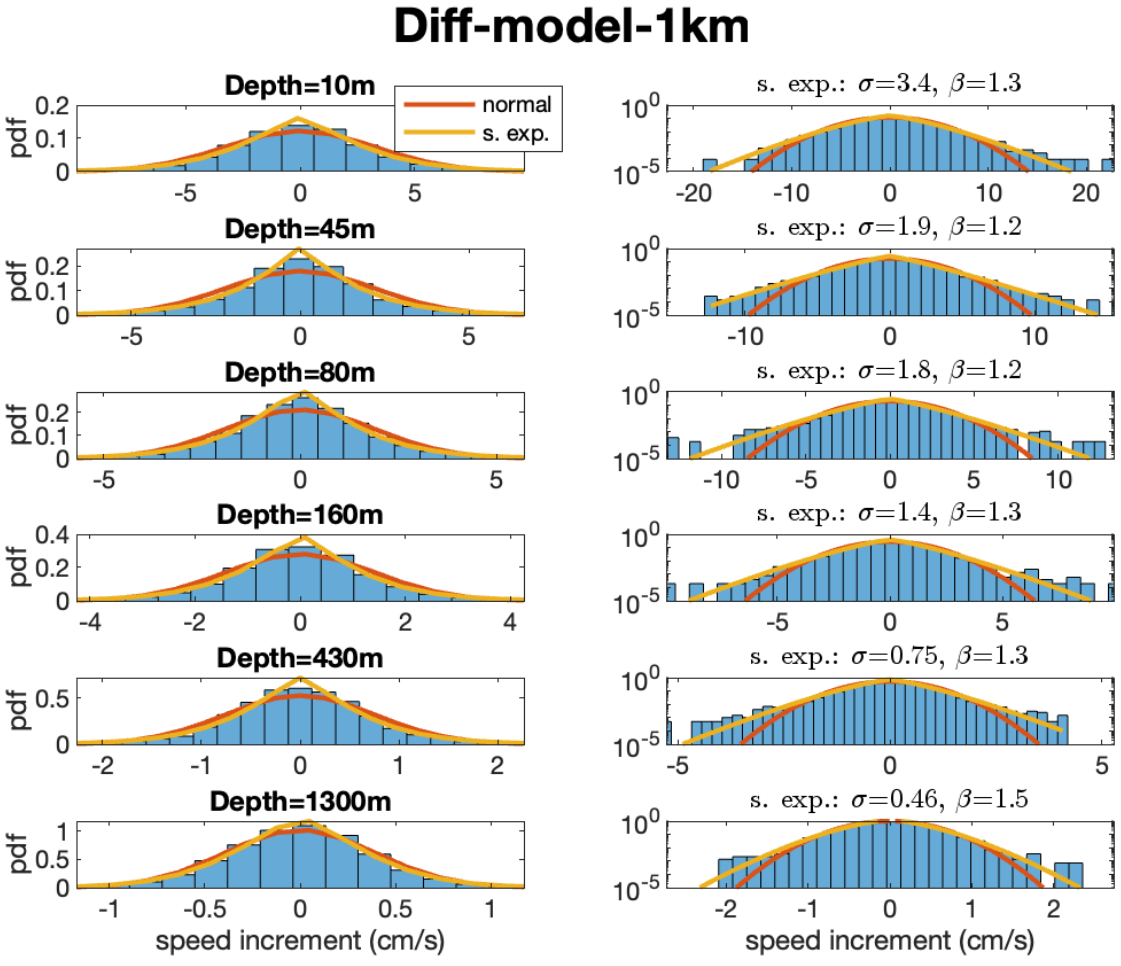

Figure A9. The pdfs of the (1 km resolution) model's current speed increment time series in regular (left panels) and semi-log (right panels) plots. The corresponding depths are indicated in the title of the left panels while the parameters of the stretched exponential distribution are indicated in the title of the right panels. The fitted normal (red) and stretched exponential (yellow) pdfs are also included. Note the smaller horizontal range of the distribution in comparison to those of the measured data (Fig. 8).

https://doi.org/10.5194/egusphere-2025-53
Preprint. Discussion started: 24 January 2025

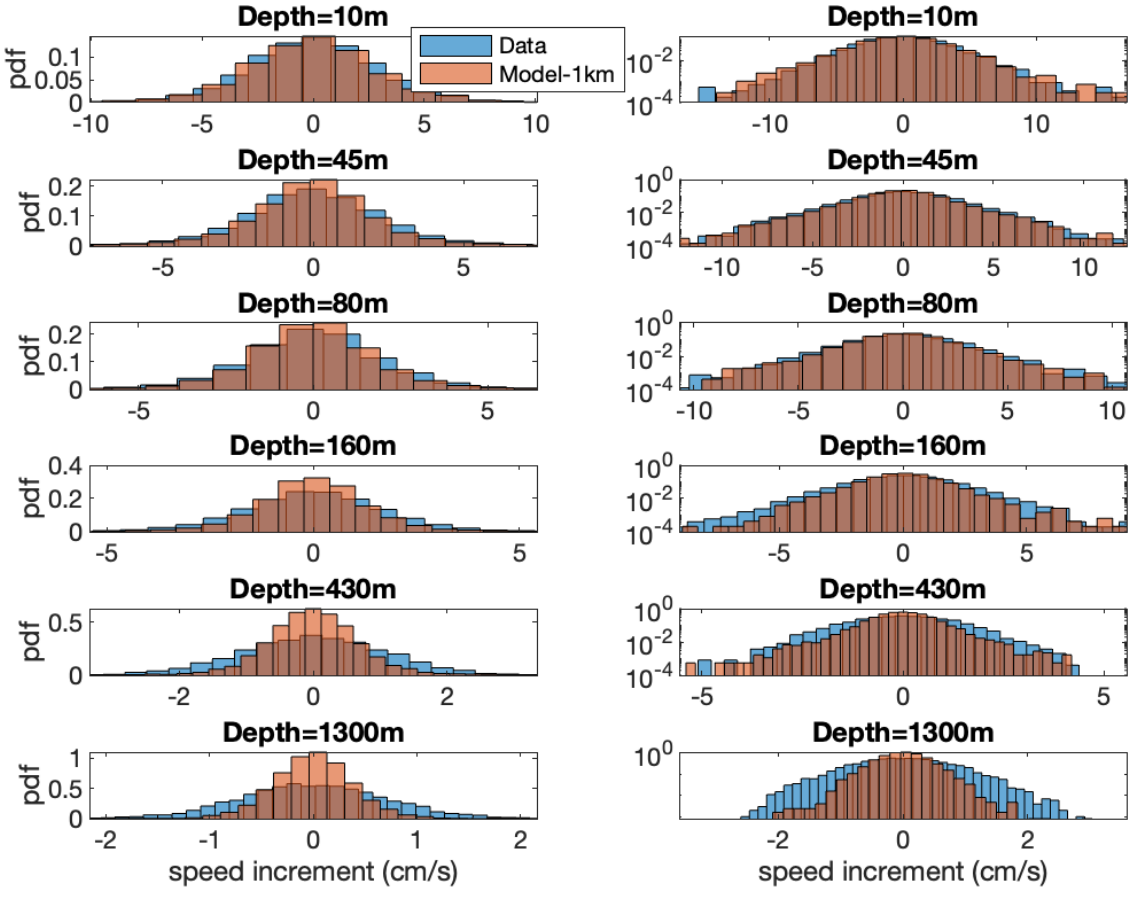

Figure A10. The data (blue) and model (light brown) pdfs of the current speed increments (two-hour resolution) in regular (left panels) and semi-log (right panels) plots for time series of the common times of the data and model. The corresponding depths are indicated in the title of the panels. The overlapping part of the pdfs is indicated by the dark brown color. Note that the tails of the data's pdfs span larger than that of the model, indicating that the speed increments of the data are larger than those of the model.

https://doi.org/10.5194/egusphere-2025-53
Preprint. Discussion started: 24 January 2025

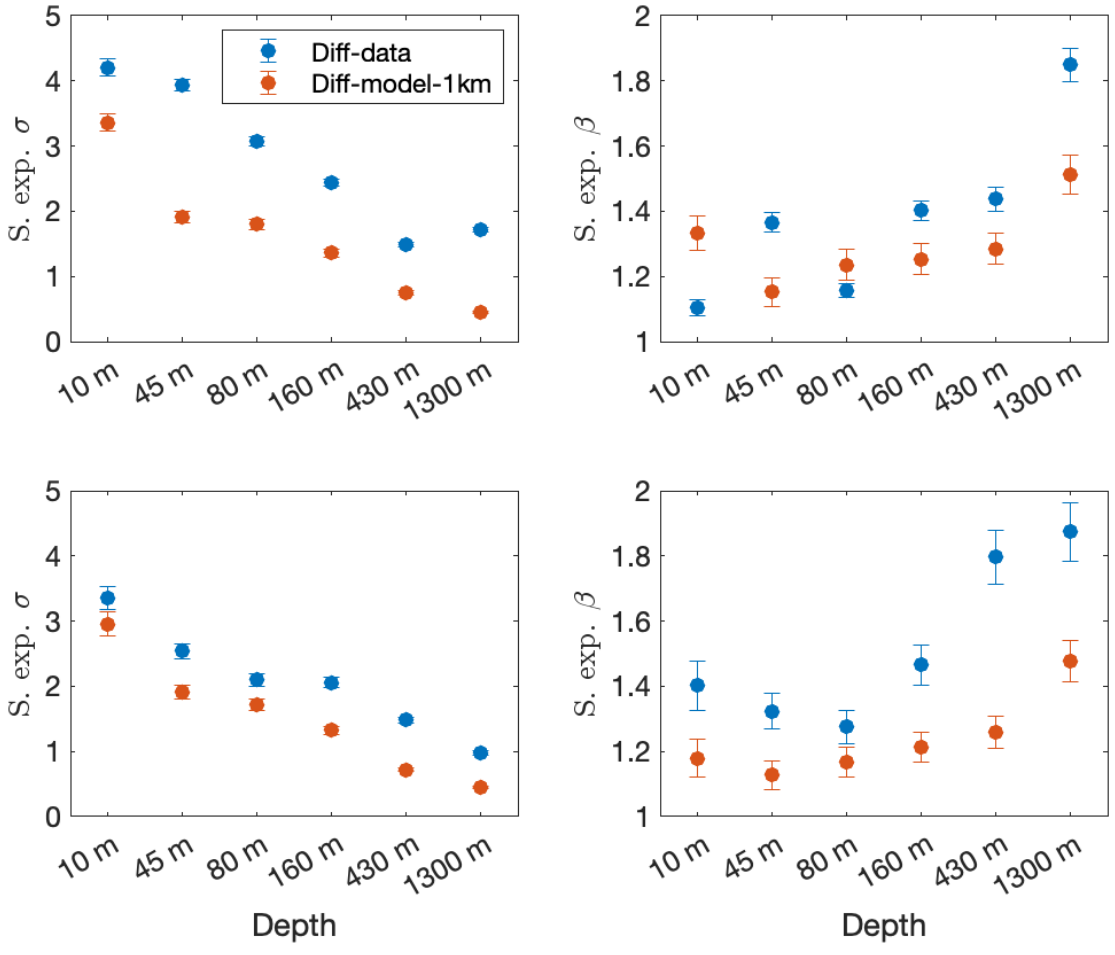

Figure A11. The estimated parameters σ (right panels) and β (left panels) of the stretched exponential pdf versus depth of the current speed increment of the data (blue circles) and 1 km resolution model (red circles). The upper panels depict the results of the original data and 1 km resolution model currents while the lower panels depict the results of time series for the common measurement times (intersection). The error bars indicate the 5-95% confidence interval (which is not always visible).

https://doi.org/10.5194/egusphere-2025-53
Preprint. Discussion started: 24 January 2025

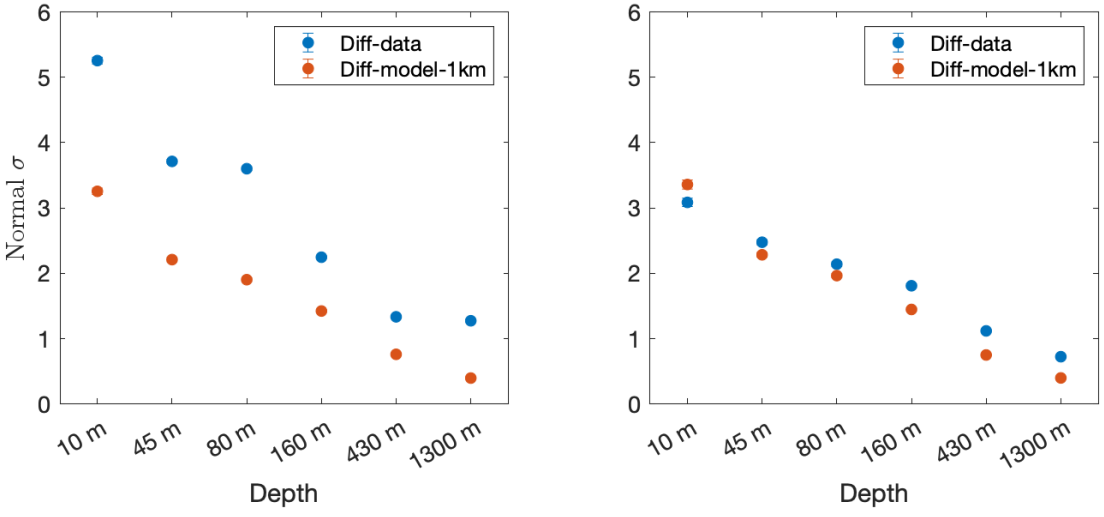

Figure A12. The estimated parameter σ normal pdf versus depth of the current speed increment of the data (blue circles) and 1 km resolution model (red circles). The left panel depicts the results of the original data and 1 km resolution model currents while the right panel depicts the results of the time series for the common measurement times (intersection). The error bars indicate the 5-95% confidence interval (which is not always visible).

https://doi.org/10.5194/egusphere-2025-53
Preprint. Discussion started: 24 January 2025

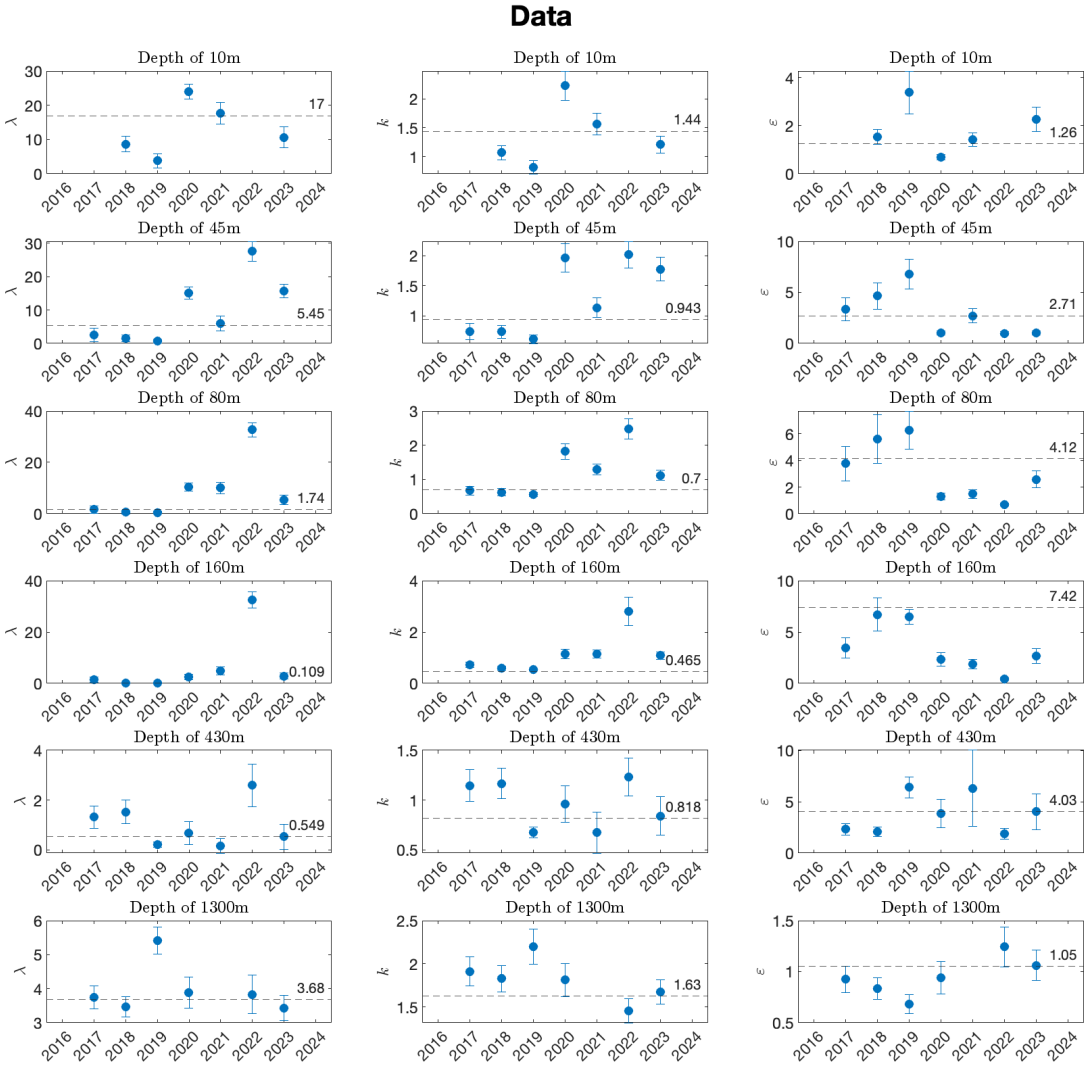

Figure A13. The annual estimated GG distribution parameters that are based on the measured current speed time series shown in Fig. 2. We show the parameters only when the number of data points spans more than half a year. The horizontal dashed lines represent the estimated parameter of the entire time series. Note that the estimated GG parameters for depths of 80 m and 160 m (third and fourth rows) are inaccurate as the MLE did not converge. The error bars indicate the 5-95% confidence interval.